Rab8-, Rab11-, and Rab35-dependent mechanisms coordinating lumen and cilia formation during Left-Right Organizer development

Abrar A. Aljiboury[1, 2, 3], Eric Ingram[1, 2, 3, 4], Nikhila Krishnan[1, 2, 3, 5], Favour Ononiwu[1, 2, 3], Debadrita Pal[1, 2, 3], Julie Manikas[2, 6], Christopher Taveras[2], Nicole A. Hall[2, 6], Jonah Da Silva[2], Judy Freshour[2, 3] and Heidi Hehnly[2, 3, *]

[1] Authors contributed equally to this work and are listed in alphabetical order.
[2] Biology Department, Syracuse University, NY, USA
[3] BioInspired Institute, Syracuse University, NY, USA
[4] Current address, Thermo Fisher, Madison, WI, USA
[5] Current address, Department of Biology, Brandeis University, MA, USA
[6] Current address, Department of Cell Biology, NYU Grossman School of Medicine, NY, USA

*Lead contact, correspondence: hhehnly@syr.edu, Twitter: @LovelessRadio

ABSTRACT

An essential process for cilia formation during epithelialization is the movement of the centrosome to dock with the cell's nascent apical membrane. Our study examined centrosome positioning during the development of *Danio rerio's* left-right organizer (Kupffer's Vesicle, KV). We found that when KV mesenchymal-like cells transition into epithelial cells that are organizing into a rosette-like structure, KV cells move their centrosomes from random intracellular positions to the forming apical membrane in a Rab11 and Rab35 dependent manner. During this process, centrosomes construct cilia intracellularly that associated with Myo-Va while the centrosomes repositioned towards the rosette center. Once the centrosomes with associated cilia reach the rosette center, the intracellular cilia recruit Arl13b until they extend into the forming lumen. This process begins when the lumen reaches an area of approximately 300 μm^2. Using optogenetic and depletion strategies, we identified that the small GTPases, Rab11 and Rab35, regulate not only cilia formation, but lumenogenesis, whereas Rab8 was primarily involved in regulating cilia length. These studies substantiate both conserved and unique roles for Rab11, Rab35, and Rab8 function in cilia formation during lumenogenesis.

INTRODUCTION

A fundamental question in cell biology is how a cilium is made during tissue formation. A primary or motile cilium is a microtubule-based structure that extends from the surface of a cell and can sense extracellular cues to transmit to the cell body. Defects in cilia formation can lead to numerous disease states collectively known as ciliopathies (Vertii *et al.*, 2015; Hall and Hehnly, 2021). Foundational studies identified two distinct pathways for ciliogenesis *in vivo* using tissues from chicks and rats (Sorokin, 1962). One mechanism for ciliogenesis which we refer to as extracellular, was found in lung cells where the centrosome first docks to the plasma membrane followed by growth of the ciliary axoneme into the extracellular space (Sorokin, 1968). The second mechanism, which we refer to as intracellular, was identified in smooth muscle cells and fibroblasts where the centrosome forms a cilia first within a ciliary vesicle in the cell cytosol before docking to the plasma membrane (Sorokin, 1962). These studies raise the possibility that different ciliated tissues construct their cilia differentially due to the nature of how a tissue develops. This presents an important hypothesis that variations in cilia formation mechanisms may occur *in vivo* during specific types of tissue morphogenesis. In our studies herein we will examine how cilia are assembled during Mesenchymal to Epithelial Transition (MET) in a vertebrate model, *Danio rerio* (zebrafish).

MET is an evolutionarily conserved process that occurs during the creation of ciliated tissues (Pei *et al*., 2019). An excellent example of this is with the vertebrate organ of asymmetry. An organ of asymmetry is required to place visceral and abdominal organs with respect to the two main body axes of the animal (Grimes and Burdine, 2017). Zebrafish is a genetically tractable model to examine how cilia form during organ of asymmetry development due to the embryo's transparency and external development. In zebrafish, the organ of asymmetry is known as the Kupffer's Vesicle (KV). KV development is easily monitored using fluorescent markers to note KV mesenchymal-like precursor cells congregating together and self-organizing into a rosette-like structure where they establish apical-basal polarity at the rosette center (Amack and Yost, 2004; L. I. Rathbun *et al*., 2020). The rosette center is the site where a fluid-filled lumen forms and KV cells will then extend their cilia into (Navis *et al*., 2013). Once KV cilia are formed

they beat in a leftward motion to direct fluid flow essential for the establishment of the embryo's left-right axis (Nonaka *et al*., 1998). While much is known about KV post-lumen formation (Amack, 2021; Grimes and Burdine, 2017; Matsui *et al*., 2015; Matsui and Bessho, 2012; Okabe *et al.*, 2008), little is known about the spatial and temporal mechanisms that regulate cilia formation during KV development.

KV formation is known to arise from a sub-population of endoderm cells. The endoderm is induced by high levels of Nodal signaling during early development that contributes to the formation of the liver, pancreas, intestine, stomach, pharynx, and swim bladder (Warga and Nüsslein-Volhard, 1999). A subset of the endoderm, called dorsal forerunner cells (DFCs) are precursors of the KV (Melby *et al.*, 1996; Essner *et al.*, 2005; Oteíza *et al.*, 2008). The number of DFCs range from 10-50 cells per embryo that can expand into >150 cells that make up the fully functional KV (Gokey *et al.*, 2016; Moreno-Ayala *et al.*, 2021). Early studies reported that these DFCs present as mesenchymal-like and are migratory. They lack clear apical/basal polarity (lack of aPKC distribution) until KV cells establish into rosette-like structures (Essner *et al.*, 2005). Apical polarity establishment of aPKC, at least in part, coincides with cystic fibrosis transmembrane conductance regulator (CFTR) accumulation at apical sites, which is a requirement for ultimate lumen expansion (Essner *et al.*, 2005; Navis *et al.*, 2013). KV cell rosette-like structures can either form as multiple cells congressing to make a single rosette or cells assembling multiple rosettes which then transition to a single rosette-like structure. The single rosette transitions into a cyst of ciliated cells surrounding a fluid-filled lumen (Essner *et al.*, 2005; Compagnon *et al.*, 2014).

One essential structure for cilia formation is the centrosome. The centrosome is commonly known as the main microtubule organizing center of the cell with two barrel shaped microtubule structures called centrioles enclosed in a network of proteins called the pericentriolar matrix (Vertii *et al.*, 2016). The position of the centrosome within the cell can be integral in generating specific cues that facilitate cellular processes such as where the apical membrane and cilium will form. In *C. elegans* intestinal cells, the placement of the centrosome during epithelialization at the apical membrane is necessary for apical membrane establishment (Feldman and Priess, 2012), but in these cells the centrosome is not destined to ever form a primary cilium. One question that arises is what molecular

and cellular mechanisms dictate when the centrosome should move to the apical membrane? Our studies herein have identified some potential mechanisms for centrosome positioning. We find that KV centrosomes reposition towards the forming apical membrane with an associated cilium in a Rab11-, but not Rab8-, dependent manner suggesting a connection between the centrosome and Rab11-endosomes that is likely important in both centrosome positioning and its ability to form a primary cilium.

While select Rab GTPases have been extensively studied, most of them have not been assigned to a detailed function or localization pattern throughout early embryonic vertebrate development. Rab GTPases comprise approximately 60 genes in vertebrates, with each Rab localizing to specific intracellular membrane compartments in their GTP-bound (active) form. These active Rabs then bind to effector proteins to aid in various steps in membrane trafficking some of which can facilitate cilia, polarity, and/or lumen formation (Borchers *et al.*, 2021; Homma *et al.*, 2021). *In vitro* assays have been used to screen the Rab GTPase family to identify which Rabs are used in lumen establishment or ciliogenesis. These screens involve the use of mammalian cell culture systems that are either depleted or genetically null for Rab GTPase family members (Yoshimura *et al.*, 2007; Oguchi *et al.*, 2020; Homma *et al.*, 2021). Some Rab GTPases identified were involved in either cilia or lumen formation, and a subset of those were involved in both such as Rab11, Rab8, and Rab35 (Bryant *et al.*, 2010; Knödler *et al.*, 2010; Westlake *et al.*, 2011; Klinkert *et al.*, 2016; Kuhns *et al.*, 2019; Naslavsky and Caplan, 2020; Belicova *et al.*, 2021). Here we investigated these three Rab GTPases in KV development. Using a combination of depletion and optogenetic clustering approaches we have identified a role for Rab11 and Rab35 in KV lumen and cilia formation, but Rab8 is only necessary in regulating cilia length. While much is known about Rab8, Rab11, and Rab35, in ciliogenesis and/or lumen formation in the context of mammalian cell culture conditions, our findings were surprising in that Rab8 did not seem to affect lumen or cilia formation where it does in mammalian cell culture (Bryant *et al.*, 2010; Knödler *et al.*, 2010; Westlake *et al.*, 2011; Naslavsky and Caplan, 2020). In this context, Rab8 and Rab11 work together in a GTPase cascade that is required for both cilia and lumen formation. However, in KV Rab8 is dispensable for lumen formation suggesting that specific cell types during potentially different developmental processes may have different

dependencies on Rab GTPases that can be identified using developmental model systems such as zebrafish.

RESULTS

KV cilia form prior to KV lumen formation.

To test when KV cells start to make cilia during KV morphogenesis, Sox17:GFP-CAAX transgenic embryos were employed to mark KV cells and fixed at different stages of KV development, pre-rosette (8-9 hours post fertilization, hpf), rosette (10 hpf), and lumen (12 hpf, Figure 1A). The pre-rosette stage is where KV cells are more mesenchymal-like and have yet to organize into a rosette, whereas in the rosette stage KV cells are organized into a rosette-like structure with their newly forming apical membranes pointed towards the rosette center (Amack and Yost, 2004; Amack *et al.*, 2007). The lumen stage is where ciliated KV cells surround a fluid filled lumen (Figure 1A). After fixing embryos at each of these stages, embryos were immunostained for centrosomes and cilia using antibodies against γ- and acetylated-tubulin (Figure 1B). A significant population of KV cells started to form cilia at the centrosome in the cell body at both the pre-rosette and rosette stage of KV development (Figure 1B-C). During the pre-rosette stage, 33.25±3.33% of KV cells had cilia; that increased to 48.06±5.94% at the rosette stage and averaged at 64.82±5.27% early on during lumen development (12 hpf, Figure 1C). These studies suggested that KV cells were forming cilia before they had an extracellular space (KV Lumen) to position into and that KV lumen formation correlated with a significant increase in KV cells having cilia.

Our findings in Figure 1B-C suggest a cellular mechanism where cilia are formed at random locales in KV cells, with cilia and associated centrosomes needing to move inside the cell towards where an apical membrane is being constructed at the rosette center. At this locale, the cilia would be positioned perfectly to extend into the lumen. To test this idea, volumetric projections of surface rendered KV cells were performed at the pre-rosette, rosette, and lumenal stages. KV cell outlines were noted using GFP-CAAX and cilia were immunostained using acetylated tubulin (Figure S1A). Surface rendering using IMARIS software allowed for the spatial positioning of cilia in KV cells across KV

developmental stages to be assessed (Figure S1A, Video S1). The boundaries of the cell (GFP-CAAX) and cilia (acetylated tubulin) were highlighted to create a three-dimensional space filling model of both cell and cilia. We identified that as KV develops from pre-rosette to rosette, to lumenal stage, intracellular cilia approach the apical membrane. Once a lumen is formed, the cilia extend into the developing KV lumen (Figure S1A). To identify if KV cell cilia were positioning towards the center of the KV cellular mass over the course of its development, we calculated the relative distance of cilia from the cell boundary closest to the KV center from the embryos shown in Figure 1B (modeled in Figure S1B; calculations in Figure 1D). When values approach 0, cilia are approaching the cell boundary closest to the KV center. This occurs significantly as KV cells transitioned from a pre-rosette organization to lumenal stages (Figure 1D), suggesting that KV cell cilia are constructed intracellularly, then positioned to the cell boundary closest to KV center where they are primed to extend their cilia into the forming lumen.

We next characterized cilia length during this process. Cilia length was measured in KV cells before lumen formation (lumen area of 0 μm^2) and at increments of lumen expansion (up to a lumen area of $5*10^3$ μm^2). Cilia in KVs with no lumen had an average length of 2.25 μm. Once a lumen starts to form, a significant increase in cilia length occurs where cilia have an average length of 4.5 μm (Figure 1E). This increase in cilia length starts when the KV lumen approaches an area of approximately 300 μm^2 and remains consistent out to $5*10^3$ μm^2 (Figure 1E). These studies suggest that cilia first form inside the cell, then position towards the rosette center where they then can extend and elongate into the KV lumen.

To confirm that cilia were forming through a potential intracellular pathway versus an extracellular pathway (modeled in Figure 1F), we immunostained for Myosin Va (Myo-Va). Class V myosins are actin-based motor proteins that have been implicated in organelle transport and tethering. Myo-Va specifically is associated with Rab11 positive membranes that move to the cell periphery and is a potential Rab11-effector protein (Lindsay *et al.*, 2013). Myo-Va has been reported to be required for the recruitment of pre-ciliary vesicles to the distal appendages of the mother centriole and can positively mark the ciliary vesicle/cap (Wu *et al.*, 2018; Ganga *et al.*, 2021). Here we used Myo-Va as a marker for the pre-ciliary vesicle and as a potential marker to denote if KV cells are

using an intracellular mechanism for cilia assembly. A space filling model for the KV cell membrane, cilia, and Myo-Va was employed to visualize cilia inside versus outside the cell (Figure 1G). Myo-Va surrounds the cilium in KV cells at a rosette stage with cilia inside the cell (Figure 1G). This finding was like that reported for *in vitro* cultured cell lines, Retinal Pigment Epithelial (RPE) and a mouse fibroblast line (NIH3T3) (Wu *et al.*, 2018). Once the cilium extended out into the lumen, Myo-Va remained at the cilium's base (Figure 1G). These studies suggest a mechanism where KV cell cilia are forming through an intracellular pathway that recruits pre-ciliary vesicles positive for Myo-Va. These Myo-Va vesicles then form a ciliary cap for the cilia to grow within. The cilia with associated cap can then fuse with the plasma membrane and KV cilia can extend into the lumen (summarized in Figure 1F).

Live embryo characterization of Rab8, Rab11, Rab35 and actin localization during KV cilia and lumen formation

Previous work in mammalian culture systems and with preliminary morpholino studies in zebrafish KV have implicated Rab8, Rab11, and Rab35 in cilia and/or lumen establishment (Bryant *et al.*, 2010; Knödler *et al.*, 2010; Westlake *et al.*, 2011; Klinkert *et al.*, 2016; Kuhns *et al.*, 2019; Naslavsky and Caplan, 2020; Belicova *et al.*, 2021). However, their cellular distribution during KV development has not been investigated, nor has it been positioned in relation to KV cilia formation or to actin recruitment to the apical membrane. Foundational studies have demonstrated that at least one of the paralogs of Rab8, Rab11, and Rab35 is broadly expressed throughout zebrafish development, including KV (Demir *et al.*, 2013; Kuhns *et al.*, 2019; Zhang *et al.*, 2019; Willoughby *et al.*, 2021). In consideration of these findings, we expressed fluorescently tagged Rab8a, Rab11a, and Rab35 by mRNA injection and assessed their distribution in the zebrafish KV marked by the plasma membrane marker GFP-CAAX (Figure 2A, 2C, 2D, S2, Video S2). In addition, we used an endogenously GFP tagged transgenic line of Rab11 (Figure 2B, (Levic *et al.*, 2021)). We identified that Rab8 was broadly recruited to the apical membrane during rosette formation and remained there during lumen opening (Figure 2A). This distribution was comparable to ectopically expressed Rab11 at the rosette stage (Figure S2A), where both Rab8 and Rab11 are recruited to the forming apical membrane

(Figure 2A, S2A). Rab11 distribution was confirmed using the endogenously tagged GFP-Rab11 line (Figure 2B). Once the lumen starts to open, Rab11 segregates towards cell-cell junctions (Figure 2B) similar to the distribution pattern of actin (labeled using Lifeact-mRuby, Figure 2C, Video S2). Expression of mRuby-Rab35 presented with localization to cell boundaries and some punctate cytosolic distribution (Figure 2D). To assess segregation of GTPases to cell-cell junctional sites noted with Rab11 and actin, the fluorescent intensity was measured between cell-cell junctional sites and the apical membrane. A ratio was calculated as junctional intensity over apical intensity (Figure 2F). We found that Rab11, Rab8, Rab35, and actin all became recruited to the apical membrane, with Rab11 and actin segregating to cell-cell junctional locales once the lumen opened when compared to Rab8 and Rab35 (Figure 2F). These findings suggest that Rab11 and actin remodeling are occurring at the apical membrane with similar timing as when the cilia should be extending into the lumen.

We next tested when KV cilia extend into the forming KV lumen. To do this we employed two strategies. We first imaged in live embryos cilia extending into the lumen using Sox17:GFP-CAAX embryos to denote the KV cells that ectopically expressed the cilia marker Arl13b-mCardinal (Figure 2E). With the second strategy we fixed GFP-CAAX embryos at various lumen sizes ranging from 0 to $5*10^3$ μm^2 and measured the percentage of KV cells that had lumenal cilia (Figure 2G). These approaches both demonstrated that cilia dock at the apical membrane during early lumen formation and then extend into the lumen (Figure 2E) once the lumen area approaches approximately 300 μm^2 (Figure 2G). When comparing these studies to when cilia start to elongate in length (Figure 1E), it suggests that cilia, when inside a KV cell, can reach a length of 2.5 μm, but once a lumen is formed (300 μm^2 in area), the cilia can extend into the lumen and grow to their final length of 4 μm. This suggests a cellular model where the intracellular KV cilia first dock at the plasma membrane, after actin and Rab11 redistribute to cell-cell junctions, and then extend into the lumen once the lumen expands to the appropriate size.

Rab11 and Rab35 modulate KV lumen formation.

Previous studies in 3D cultures of Madin-Darby canine kidney (MDCK) cells (cysts) (Bryant *et al.*, 2010) implicated that the small GTPase Rab11 acts upstream of Rab8 in a GTPase cascade needed for appropriate lumen formation. Interestingly, an additional Rab GTPase, Rab35, was also implicated in lumen opening using this same 3D culture system (Klinkert *et al.*, 2016). Here we tested the requirement of Rab11, Rab8, and Rab35 on KV lumen establishment using two strategies, morpholino (MO) transcript depletion using MOs that have been previously characterized ((Omori *et al.*, 2008; Westlake *et al.*, 2011; Kuhns *et al.*, 2019), Figure S3A) and an acute optogenetic clustering strategy (Figure 3A). The optogenetic strategy causes an acute inhibition of Rab11-, Rab8-, and Rab35-associated membranes through a hetero-interaction between cyptochrome2 (CRY2) and CIB1 upon exposure to blue light during specific KV developmental stages (Figure 3A, (Nguyen *et al.*, 2016; Rathbun *et al.*, 2020b; Krishnan *et al.*, 2022)). With acute optogenetic clustering of Rab11- and Rab35-associated membranes and with depletion of Rab11 and Rab35 transcripts using MOs, we found severe defects in lumen formation (Figure 3B-D, S3B-F) when comparing to control conditions (CRY2, Figure S3C; control MO, S3D-E). This was measured both by following lumen formation live using an automated fluorescent stereoscope set up for a set time frame (Figure 3B, S3C) and at a fixed developmental endpoint (6 SS, 12 hpf, Figure 3D, S3D-F). Sox17:GFP-CAAX marked KV cells were used to assess lumen formation. Zebrafish embryos were imaged just past 75% epiboly for over 4 hours, during this time, the Rab35 and Rab11 clustered embryos that were imaged were not able to form a lumen when compared to control (CRY2, Figure 3B-D, S3C, Video S3). To characterize KV developmental defects with acute clustering of Rab8, Rab11, and Rab35, KV morphologies were characterized at a fixed developmental endpoint (6SS, 12 hpf). We found that Rab11 and Rab35 clustered embryos presented with defects in forming a rosette (42.5% of embryos for Rab11, 28.1% for Rab35) or transitioning from a multiple rosette state to a single rosette state (37.5% of embryos for Rab11, 18.5% for Rab35, Figure 3D, Video S3 and Figure 3B for Rab35 clustering) compared to CRY2 embryos or Rab8 clustered embryos (100% form lumen, Figure 3D, Video S3). Interestingly, Rab35-clustered embryos were able to form separate rosettes that were not in the same cellular KV mass and in some cases

one of the rosettes could transition to a small KV structure with a lumen (refer to Figure S3F, counts in Figure 3D). While a Rab11-Rab8 GTPase cascade during lumen formation has been proposed in the context of mammalian cell culture conditions (Bryant *et al.*, 2010), our findings were surprising in that acute Rab8 clustering conditions or Rab8 depletion conditions by MO does not affect lumen formation during KV development, but instead Rab11 and Rab35 play a predominant role. The comparison of *in vivo* to *in vitro* systems suggested to us that specific cell types during potentially different developmental processes may have different dependencies on the Rab GTPase family.

Optogenetic clustering of Rab8, Rab11, and Rab35 present unique roles in regulating actin and CFTR cellular distribution.

Since both Rab11 and Rab35 optogenetic clustering, but not Rab8, resulted in lumen formation defects we wanted to examine whether they disrupted two pathways that have both been implicated in regulating KV lumen formation: CFTR recruitment to the apical membrane (Navis *et al.*, 2013) and actin dynamics (Wang *et al.*, 2011; Saydmohammed *et al.*, 2018). CFTR is a master regulator of fluid secretion into lumenal spaces. CFTR is transported through the secretory pathway to the apical membrane where it mediates chloride ion transport from inside the cell to outside the cell. Loss of CFTR-mediated fluid secretion impairs KV lumen expansion leading to laterality defects (Navis *et al.*, 2013). Actin based molecular motors, Myosin1D (Saydmohammed *et al.*, 2018) and Myosin II (Wang *et al.*, 2011), and a known actin regulator, Rho associated coiled-coil containing protein kinase 2 (ROCK2, (Wang *et al.*, 2011)), have been implicated in establishing LR asymmetry. In our studies we found that Rab11 optogenetic clustering causes a severe defect in the delivery of CFTR to the apical membrane where CFTR-GFP becomes trapped in Rab11-clustered membrane compartments (Figure 4A, 4C). Rab35 optogenetic clusters also partially contain CFTR (Figure 4A, 4C), but not to the same extent as Rab11-clustered membranes. With both Rab11 and Rab35 clustering, there was significantly less CFTR that was able to be delivered to forming apical membranes. This is consistent with defects in KV rosette and lumen formation observed with Rab35 and Rab11 clustered embryos (Figure 3D). Interesting, some Rab35 clustered embryos demonstrate multiple rosettes that form in a KV, with one rosette being

competent for lumen formation but defective in expansion (Figure 4A). When this occurs, we find that the rosette that is competent in opening has CFTR localized to the apical membrane (Figure 4A), as opposed to the secondary rosette that cannot open (Figure 4A, inset). No defect in CFTR delivery to the apical membrane was noted with Rab8 optogenetic clustering (Figure 4A, 4C), consistent with the lack of observed defects in lumen formation with both optogenetic clustering (Figure 3D) and depletion of Rab8 using morpholinos (Figure S3D-E).

Actin organization was significantly disrupted in embryos with optogenetically clustered Rab11 (Figure 4B, 4D), but not in Rab8 or Rab35 optogenetic conditions. Under control conditions (Figure 2), we found that Rab11 and actin distributed from broad apical membrane localization during the rosette stage of KV development to cell-cell junctions during lumen formation and expansion (Figure 2B, 2C), whereas Rab35 and Rab8 had more even distribution at cell boundaries and across the apical membrane respectively (Figure 2A, 2D, 2F). When Rab11 membranes were optogenetically clustered, a robust recruitment of actin was associated with these membranes compared to Rab8 or Rab35 clustered membranes (Figure 4B, 4D). Together these studies suggest that Rab11 and Rab35 may be working together for CFTR delivery to the apical membrane to initiate lumen expansion, but that Rab11 has a likely role in actin remodeling independent of Rab35.

Some GTPases are known to work together on the same membrane compartment. For instance, Rab11 and Rab8 were reported to function together in a GTPase cascade in cellular events such as lumen formation and ciliogenesis. In this situation, Rab11 acts upstream of Rab8 by recruiting the Guanine Exchange Factor (GEF) for Rab8, Rabin8 (Bryant *et al.*, 2010; Knödler *et al.*, 2010; Westlake *et al.*, 2011). Based on our findings that both Rab11 and Rab35 cause defects in lumen formation (Figure 2) and CFTR trafficking (Figure 4A, 4C), we asked if Rab11, Rab35, and/or Rab8 could act on the same membrane compartment. To test this, we performed optogenetic clustering of Rab35 or Rab11 and determined whether clustering one recruited Rab11, Rab35, or Rab8. Optogenetic clustering of Rab11 resulted in the recruitment of Rab8 but not Rab35 (Figure 4E, 4F). This is consistent with the idea that a Rab11 cascade may still exist between Rab11 and Rab8, but that this cascade may not be needed for CFTR transport

or KV lumen formation. It also suggests that Rab11 is not acting upstream of Rab35. Interestingly, upon optogenetic clustering Rab35 membranes, Rab11 becomes significantly co-localized (Figure 4E, 4F) suggesting that Rab35 may act upstream of Rab11. In summary, we find that Rab35 and Rab11 may work together to ensure appropriate lumen formation through managing CFTR trafficking to the forming apical membrane (Figure 3, 4).

Rab11 and Rab35 associated membranes are needed for KV cilia formation and extension into the lumen, whereas Rab8 is needed for cilia length regulation.

Our initial studies demonstrated that KV cilia extend into the lumen once the lumen reaches an area 300 μm^2 (Figure 2G). Then KV cilia can reach their maximum length of approximately 4 μm (Figure 1E). These findings suggested that mechanisms regulating lumen formation involving the GTPases Rab11 and Rab35, may also play an important role in coordinating cilia formation. To explore this idea, we examined the localization of Rab11 and Rab35, along with Rab8, in relation to KV cilia (Figure 5A). We used the endogenously tagged GFP-Rab11 zebrafish line and ectopically expressed mRuby-Rab35 (Figure 5A, S4A-B). Embryos were fixed at the KV rosette stage (Figure 5A, top) and lumen stage (Figure 5A, bottom), and cilia were immunostained for acetylated tubulin. When imaging the KV rosette stage, we found that cilia were organized intracellularly surrounded by Rab11 membranes that were organized at the center of the rosette, while Rab8 was organized at the base of the cilia where the centrosome resides (Figure 5A). As the KV develops to a lumen stage, Rab11 reorganizes to the base with Rab8 (Figure 5A). Throughout the developmental stages Rab35 organized to cell boundaries (Figure 2D, S4B) with no specific localization to the cilia itself (Figure S4B). To test the requirement of Rab11, Rab8, and Rab35 on KV cell cilia formation and/or centrosome positioning we employed two strategies, MO transcript depletion (Figure S3A, S4C) and the acute Rab GTPase optogenetic clustering assay (modeled in Figure 3A). Our studies found that optogenetically clustering Rab11- or Rab35-membranes during early KV development caused a significant decrease in the percentage of KV cells that could form cilia (Figure 5B, 5D). When comparing Rab11, Rab8, and Rab35 clustered embryos to control (CRY2 injected), we identified that only 35.81±8.79% of Rab11 and 49.72±5.50%

of Rab35 clustered KV cells were able to make a cilium compared to Rab8 clustered (64.43±3.85%) and CRY2 controls (78.03±3.86%, Figure 5B, 5D). These findings were surprising in that it suggested that Rab11- and Rab35-associated membranes, but not Rab8, were required for KV cilia formation. However, clustering Rab11 and Rab35 also produced more severe defects in KV lumen formation (Figure 3), suggesting that their role may be to coordinate both lumen and cilia formation to occur at the appropriate time during KV development.

We next wanted to test in the cells that could make cilia, whether the cilia were abnormal in length. In addition, we examined in the KVs that formed lumen whether cilia could extend into it. Rab11, Rab8, and Rab35-clustered cells that made cilia demonstrated significantly decreased cilia length (2.92±0.14 μm for Rab11, 3.15±0.08 μm for Rab8, and 2.02±0.05 for Rab35) compared to control CRY2 conditions (4.13±0.06 μm, Figure 5E). This significant decrease in cilia length with Rab11, Rab8, and Rab35 clustering, is consistent with Rab11, Rab8, or Rab35 depletion using morpholinos (Figure S4C, (Westlake *et al.*, 2011; Lu *et al.*, 2015; Klinkert *et al.*, 2016)). Interestingly, Rab8 clustering did cause a significant decrease in cilia length (Figure 5E), but not in the formation of cilia or lumen (Figure 3B-D, 5C). This suggests that Rab8 may have a more direct role in cilia function and not in lumen formation. We next examined if the cilia that were made were stuck in the cell volume. In Rab11 (20.59±5.34%) and Rab35 clustered KV cells (26.02±5.25%) had cilia stuck within the cell volume compared to Rab8 clustered cells (2.32±1.45%) or CYR2 controls (5.44±1.69%, Figure 5F). These findings suggest that centrosomes that construct a cilium under Rab11- and Rab35-clustering conditions are unable to extend the cilium into the lumen and that this could be the underlying reason for cilia being significantly shorter in length. One possibility for cilia being stuck within the cell volume is that KV lumens are not able to expand beyond 300 μm^2 in area under conditions of Rab11- and Rab35- clustering (Figure 3B-D), but an additional possibility is that the centrosome and the forming cilium are unable to relocate towards the center of the KV cell mass where the rosette center and subsequent lumen will form. To test the role of Rab35-, Rab11- and Rab8-membranes in centrosome positioning during KV development, centrosome distances from the plasma membrane closest to KV center were measured under clustered conditions and compared to control conditions (CRY2,

modeled in Figure S1B). If centrosomes are positioning towards the KV center, then the number should approach 0. Rab11- and Rab35-clustered embryos measurements averaged around 0.70±0.10 and 0.75±0.11 respectively, whereas with Rab8 clustered and control conditions the centrosome distance approached 0 with a value of 0.23±0.06 and 0.30±0.03 (Figure 5G). These studies suggest that Rab11 and Rab35 coordinate lumen formation and centrosome positioning during cilia formation.

Acute optogenetic disruption of Rab8, Rab11, and Rab35 membranes during KV development results in left-right asymmetry defects.

The consequences associated with KV lumen expansion and cilia formation can have downstream developmental defects that include defects in the left-right development of the brain, heart, and gut (Grimes and Burdine, 2017). Based on this, we wanted to examine the developmental defects associated with acute optogenetic clustering of Rab8-, Rab11-, or Rab35-associated membranes during KV development (Figure 6A). Embryos expressing CIB1-Rab8, -Rab11, or -Rab35 with CRY2 were exposed to blue light to induce clustering at 75% epiboly when KV precursor (Dorsal Forerunner) cells are first visualized until 6 SS (12 hpf) when KV lumen is opening. At 6 SS blue light was removed and the embryos were left to develop to high pec (42 hpf). Gross phenotypes observed with animals having Rab8-, Rab11-, or Rab35-optogenetically clustered membranes included a significant increase in animals with curved tails. Rab35 clustering specifically resulted in a significant increase of animals displaying no tails and/or a one-eye phenotype when compared to control conditions (CRY2, Figure 6B-C). We specifically examined heart development since the heart is the first organ that is formed during zebrafish development and its laterality can be easily assessed in live embryos (Figure 6D). Using a cmlc2:GFP transgenic line to label zebrafish heart cells specifically, we assessed the process of heart looping. Abnormal heart looping includes reversed looping, no loop, or bilateral heart looping (Figure 6D-E, Video S4). Over 70% of animals presented with abnormal heart looping when Rab8-, Rab11-, or Rab35- was acutely clustered during KV developmental stages compared to control animals expressing CRY2 (13.55±1.59%). While this was not surprising for Rab11 and Rab35 optogenetic clustering during KV development due to embryos presenting with severe lumen and cilia formation

defects (Figure 3, 5), this was surprising for Rab8 optogenetic clustering conditions where embryos formed normal lumens but had shorter cilia (Figure 5E). This suggests that even subtle defects in cilia length and potential function during KV development may result in significant developmental defects. Taken together, these studies propose that Rab8-, Rab11-, and Rab35-mediated membrane trafficking is necessary for forming a functional KV during development.

DISCUSSION

Our studies focused on the Rab GTPases— Rab8, Rab11, and Rab35 —that have been linked to lumen and cilia formation in mammalian cell culture models (Bryant *et al.*, 2010; Knödler *et al.*, 2010; Westlake *et al.*, 2011; Klinkert *et al.*, 2016). We identified that during the KV pre-rosette stage, cells start to assemble a cilium inside the cell at random locales that is positive for the ciliary vesicle marker Myo-Va (Figure 1B, 1G). The cilium and associated centrosome are repositioned inside the cell towards the center of the KV cell mass at a similar time KV cells are rearranging into a rosette like structure that then transitions into a group of cells surrounding a fluid-filled lumen (Figure 1B, 1D). Once the lumen reaches a set area (300 μm^2), the KV cell cilia extend into the lumen from a location marked by Rab8 and Rab11, but not Rab35 (Figure 5A, S4A-B). We identified that Rab11- and Rab35-associated membranes are both required to mediate KV cells transition into a rosette cellular arrangement and then into a cyst of cells organized around a central lumen (Figure 3). Rab11 likely does this through mediating both actin dynamics and CFTR transport to the apical membrane (Figure 4A-D), where Rab35 may act upstream of Rab11 membranes (Figure 4E-F).

Interestingly, the only significant defect we identified with acute disruption of Rab8 was cilia length (Figure 5E), whereas with Rab11 and Rab35 we found defects in KV development that included rosette formation and transition to forming a lumen, along with a loss of cilia formation. This was surprising due to previous reports identifying a GTPase cascade between Rab11 and Rab8 that was needed for lumen formation and for cilia formation in mammalian tissue culture (Bryant *et al.*, 2010; Knödler *et al.*, 2010; Westlake *et al.*, 2011; Lu *et al.*, 2015; Cuenca *et al.*, 2019). While we argue that this cascade may not be required for lumen or cilia formation in KV cells, it may still be intact in regulation

of cilia length (Figure 5E). Our findings demonstrate that both conserved and divergent mechanisms are likely involved in cilia formation dependent on the developmental requirements of the tissue being formed. For instance, there may be a possible connection between Rab35 and Rab11, where both Rab35 and Rab11 clustered membranes result in the sequestration of CFTR, and that Rab35 clustering results in the partial recruitment of Rab11. Our findings suggest a possible connection between Rab35 and Rab11 that is coordinated during cilia and lumen formation. Interestingly, there is no colocalization with Rab35 and cilia, unlike Rab11. One potential unique mechanistic possibility is that Rab35 and Rab11 work together in coordinating lumen formation through CFTR transport. In this scenario, Rab11 or Rab35 clustering may prevent CFTR from accumulating appropriately at the apical membrane, resulting in incomplete lumen formation and cilia assembly. An additional more conserved mechanism for Rab11, similar to what is reported in mammalian cell culture, is a direct role at the cilium where Rab11 localizes to (Figure 5A). In this scenario, Rab11 can regulate cilia formation and potential elongation in a cascade with Rab8. Our findings suggest potential conserved but also unique mechanistic contributions of Rab GTPases in coordinating lumen formation and ciliation for tissues *in vivo,* leaving ample opportunity for further investigation.

ACKNOWLEDGEMENTS

We thank the Michel Bagnat lab at Duke University School of Medicine for sharing their eGFP-Rab11 transgenic zebrafish lines. This work was supported by National Institutes of Health grants R01GM127621 (H.H.) and R01GM130874 (H.H.). This work was supported by the U.S Army Medical Research Acquisition Activity through the FY16 Prostate Cancer Research Programs under Award no. W81XWH-20-1-0585 (H.H.). Opinions, interpretations, conclusions, and recommendations are those of the authors and not necessarily endorsed by the Department of Defense.

AUTHOR CONTRIBUTIONS

A.A., D.P., J.S., H.H., N.K., J.M., C.T., E.I., N.A.H and F.O. designed, performed, and analyzed experiments; H.H. wrote manuscript; J.F. provided molecular reagents and zebrafish husbandry. All authors provided edits. H.H. oversaw project.

DECLARATION OF INTERESTS

The authors declare no competing interests.

FIGURE LEGENDS

Figure 1. *KV cilia form prior to KV lumen formation using an intracellular pathway.* (**A**) Model depicting KV developmental stages: pre-rosette, rosette and lumen. Number of hours post fertilization (hpf) shown. (**B**) Confocal micrographs of KV developmental stages with cilia (acetylated-tubulin, cyan), centrosome (γ-tubulin, magenta), and actin (phalloidin, gray). Scale bar, 10 μm. (**b'**) Magnified insets from (**B**) depicting centrosome and cilia positioning in KV cells at different KV developmental stages. Bar, 7 μm. (**C**) Percentage of ciliated KV cells at the different KV developmental stages. (**D**) Relative distance of cilia from cell border closest to KV center. (**C-D**) Shown as a violin plot with median (yellow line). One way ANOVA across KV developmental stages, n>7 embryos, **p<0.01. (**E**) Scatter plot depicting average cilia length within KV cells per embryo across n=29 embryos in relation to lumen area. Error bars, ± SEM. (**F**) Model demonstrating intracellular versus extracellular pathways for cilia formation. (**G**) 3D surface rendering of representative KV cells with cilia (acetylated-tubulin, cyan) inside versus outside of KV plasma membranes (KV membranes, Sox17:GFP-CAAX, gray), Myo-Va (magenta). Bar, 5 μm. Please refer to Table S1 for additional statistical information.

Figure S1. *KV cilia form prior to KV lumen formation using an intracellular pathway.* (**A**) 3D surface rendering of a representative KV cell during pre-rosette, rosette, and lumen KV developmental stages with cilia (acetylated-tubulin, cyan) and KV plasma membranes (KV membranes, Sox17:GFP-CAAX, gray) rendered. Refer to Video S1. Bar, 5 μm. (**B**) Model depicting quantification of relative distance of the cilium from the cell border closest to KV center. Cilia, cyan. Nucleus, gray. Center of KV cells, yellow. Pink dashed line is distance of cilium from cell membrane. Black dashed line is distance of cell center to cell membrane.

Video S1. *KV cilia form prior to KV lumen formation using an intracellular pathway.* 3D surface rendering from Figure S1A of a single KV cell at the KV pre-rosette, rosette, or

lumen stage rotated 360 degrees around the X-axis. Bar, 5 μm. Inset shows full KV with cilia (cyan) and KV plasma membrane (Sox17:GFP-CAAX). Refer to Figure S1A.

Figure 2. *Live embryo characterization of Rab8, Rab11, Rab35 and actin localization during KV cilia and lumen formation.* (**A-D**) Live confocal videos of mRuby-Rab8 (cyan, **A**), GFP-Rab11 (gray, **B**), actin (lifeact-mRuby, magenta, **C**), and mRuby-Rab35 (gray, **D**) localization in KV cells during lumen formation. Refer to Video S2. Scale bar, 10μm. (**E**) KV cell building and extending a cilium (Arl13b-mCardinal) into the lumen of the KV. KV plasma membranes (Sox17:GFP-CAAX) shown (inverted gray, A,C; cyan, E). Bar, 5 μm. (**F**) Ratio of junctional to apical Rab8 (cyan), Rab11 (blue), actin (magenta) and Rab35 (purple) at the rosette, early lumen, and late lumen stages of KV development. Error bars represent ±SEM for n>4 cells. (**G**) Scatter plot demonstrating the percentage of KV cells with lumenal cilia per embryo in relation to KV lumen area. n=29 embryos. Goodness of fit R2= 0.8577. Please refer to Table S1 for additional statistical information.

Figure S2. *Live embryo characterization of Rab8, Rab11, Rab35 and actin localization during KV cilia and lumen formation.* Live confocal videos of mCherry-Rab11 (cyan) localization in KV cells during lumen formation. KV plasma membrane noted with GFP-CAAX (inverted gray). Scale bar, 10 μm. Refer to Figure 2A-D.

Video S2. *Live embryo characterization of Rab8, Rab11, Rab35 and actin localization during KV lumen formation.* Live confocal videos of actin (lifeact-mRuby, magenta), mRuby-Rab8 (cyan), GFP-Rab11 (gray), and mRuby-Rab35 (gray) localization in KV cells during lumen formation. KV plasma membranes (Sox17:GFP-CAAX) shown with actin and Rab8 (inverted gray). Bar, 10 μm. Refer to Figure 2A-D.

Figure 3. *Rab11 and Rab35 modulate KV lumen formation.* (**A**) A model depicting the use of optogenetics to acutely block Rab-associated trafficking events during KV developmental stages. (**B**) Optogenetic clustering of Rab11 and Rab35 blocks KV lumen formation compared to Rab8. Imaged on an automated fluorescent stereoscope.

Bar, 50 μm. KV marked with Sox17:GFP-CAAX, lumens highlighted in orange, clusters shown in cyan. Refer to Video S3. (**C**) KV lumen area over time (±SEM for n=3 embryos per condition). (**D**) KV morphologies measured from optogenetically-clustered then fixed embryos at 12 SS (12 hpf). n>27 embryos measured across n>3 clutches per condition. Please refer to Table S1 for additional statistical information.

Figure S3. *Rab11 and Rab35 modulate KV lumen formation.* (**A**) Agarose gel demonstrating RT-PCR of Rab8, Rab11, and Rab35 MO treatment compared to control MO conditions. Amplification of Rab8, Rab11, and Rab35 shown. NC, negative control. (**B**) Violin plot depicting lumen area from Rab8, Rab11, and Rab35 clustering conditions normalized to uninjected control values. Dots represent individual KV values. Median denoted by line. One-way ANOVA with Dunnett's multiple comparison test, compared to CRY2. n>9 embryos, ****p<0.0001. (**C**) Control CRY2 conditions from Figure 3B. Imaged on an automated fluorescent stereoscope. Bar, 50 μm. KV marked with Sox17:GFP-CAAX, lumens highlighted in orange, clusters shown in cyan. (**D**) Representative 3D rendering of KV under Rab8, Rab11, and Rab35 MO treatment. Lumen trace (orange), cell membrane (GFP-CAAX), inverted LUT), and actin (magenta) shown. Bar, 100 μm. (**E**) Violin plot depicting lumen area normalized to uninjected control values. Dots represent individual KV values. Median denoted by line. One-way ANOVA with Dunnett's multiple comparison test, compared to CRY2. n>12 embryos, ****p<0.0001. (**F**) Representative image of optogenetic clustering of Rab35 (cyan) in KV cells corresponding with Figure 3D. CFTR-GFP (grey) shown. Bar, 100 μm. Statistical results detailed in Table S1.

Video S3. *Rab11 and Rab35 modulate KV lumen formation.* Optogenetic clustering of Rab11 and Rab35 blocks KV lumen formation compared to Rab8. Embryos imaged on automated fluorescent stereoscope every 10 min. Bar, 100 μm. KV marked with Sox17:GFP-CAAX. Refer to Figure 3B.

Figure 4. *Optogenetic clustering of Rab8, Rab11, and Rab35 present unique roles in regulating actin and CFTR cellular distribution.* (**A-B**) Optogenetic clustering of Rab11,

Rab8, and Rab35 (cyan) in KV cells. Localization with CFTR-GFP (magenta, **A**) or actin (phalloidin, magenta, **B**) demonstrated in magnified insets. Bar, 7 μm. (**C-D**) Percent of optogenetic clusters that colocalize with CFTR (**C**) or actin (**D**). n>9 embryos, **p<0.01, ****p<0.0001. (**E**) Optogenetic clustering of Rab11 and Rab35 (cyan) in KV cells. Rab11 clusters localization with Flag-Rab8 (magenta) or mRuby-Rab35 shown, along with Rab35 clusters with GFP-Rab11. Bar, 7 μm. (**F**) Percent of optogenetic clusters that colocalize with Rab8, Rab35, or Rab11 was calculated. n>9 embryos, ****p<0.0001. (**C, D, F**) Statistical results detailed in Table S1.

Figure 5. *Rab11 and Rab35 associated membranes are needed for KV cilia formation and extension into the lumen, whereas Rab8 is needed for cilia length regulation.* (**A**) Confocal micrographs of KV developmental rosette stage (top) and lumen stage (bottom) with cilia (acetylated-tubulin, gray), GFP-Rab11 (cyan), and mRuby-Rab8 (magenta) shown. Bar, 10 μm. (**B-C**) Confocal micrographs of cilia (acetylated tubulin, cyan) in CRY2 (control), Rab8-, Rab11-, and Rab35-clustered Sox17:GFP-CAAX embryos (gray). Centrosomes denoted by γ-tubulin (magenta, **C**). Clusters not shown. (**B**) Lumen outline is orange dashed lines. Bar, 10 μm. (**C**) Yellow dashed lines, KV cell membranes. Orange arrow, centrosome. Bar, 2μm. (**D-G**) Violin plots of percentage of KV cells with cilia (**D**), cilia length (**E**), percentage of KV cilia in cell volume (**F**), and the relative distance of cilia from the cell boarder closest to KV center (**G**). One way ANOVA with Dunnett's multiple comparison to CRY2 (control) was performed. n>4 embryos. **p<0.01, ***p<0.001, ****p<0.0001. Statistical results detailed in Table S1.

Figure S4. *Rab11 and Rab35 associated membranes are needed for KV cilia formation and extension into the lumen, whereas Rab8 is needed for cilia length regulation.* (**A-B**) Confocal micrographs of KV lumen stage with cilia (acetylated-tubulin, cyan), GFP-Rab11 (magenta, **A**), mRuby-Rab8 (yellow, **A**), mRuby-Rab35 (magenta, **B**), and actin (yellow, **B**). Bar, 2 μm. (**C**) Violin plot of cilia length following morpholino depletion. One way ANOVA with Dunnett's multiple comparison to control was performed. n>3 embryos. ****p<0.0001.

Figure 6. *Acute optogenetic disruption of Rab8, Rab11, and Rab35 membranes during KV development results in left-right asymmetry defects.* (**A**) A model depicting the use of optogenetics to acutely block Rab-associated trafficking events during KV developmental stages and assessment of downstream developmental consequences at 42 hpf. (**B**) Images demonstrate characterized developmental phenotypes observed that include curved tail, no tail, and single eye. Yellow arrows point to abnormalities. Bar, 100 µm. (**C**) Violin plot displaying percentage of embryos displaying a no tail, curved tail, or single eye phenotype (shown in (**B**)) over n>3 clutches across the optogenetic clustering conditions compared to control. *p<0.05, and **p<0.01. (**D**) Images demonstrate characterized abnormal heart looping in clustered embryos compared to normal leftward heart looping in control CRY2 embryos. Refer to Video S4. Bar, 100 µm. (**E**) Violin plot displaying percentage of embryos with abnormal heart looping (shown in (**D**)) n>3 clutches across the optogenetic clustering conditions compared to control. ***p<0.001 and ****p<0.0001. (**C, E**) Statistical results detailed in Table S1.

Video S4. *Acute optogenetic disruption of Rab8, Rab11, and Rab35 membranes during KV development results in left-right asymmetry defects.* Stereo microscope video showing ventral view of a 48 hpf cmlc2:GFP (green) fish marking the heart. In CRY2 control, heart tube loops to the left. Rab8-, Rab11-, and Rab35- optogenetic clustered zebrafish reveal defective heart loop phenotype from Figure 6D. Size bar, 100 µm. 0.25s time interval.

EXPERIMENTAL PROCEDURES

Resource Availability

Lead contact: For further information or to request resources/reagents, contact Lead Contact, Dr. Heidi Hehnly (hhehnly@syr.edu)

Materials availability: New materials generated for this study are available for distribution.

Data and code availability: All data sets analyzed for this study are displayed.

Experimental model and subject details

Fish Lines

Zebrafish lines were maintained using standard procedures approved by Syracuse University IACUC (Institutional Animal Care Committee) (Protocol #18-006). Embryos were raised at 28.5^{o}C and staged (as described in (Kimmel *et al.*, 1995)). Wildtype and/or transgenic zebrafish lines used for live imaging and immunohistochemistry are listed in key resource table (Table S2).

Method Details

Antibodies

Antibody catalog information used in mammalian cell culture and zebrafish embryos are detailed in key resource table (Table S2).

Plasmids and mRNA

Plasmids were generated using Gibson cloning methods (NEBuilder HiFi DNA assembly Cloning Kit) and maxi-prepped before injection and/or transfection. mRNA

was made using mMESSAGE mMACHINE™SP6 transcription kit. See key resource table for a list of plasmid constructs and mRNA used.

Morpholinos

Morpholinos (MO) were ordered from Gene Tools. Previously characterized Rab8, Rab11, and Rab35 MO sequences were used from (Westlake *et al.*, 2011; Lu *et al.*, 2015; Kuhns *et al.*, 2019). See Supplementary key resource table in Table S2 for a list of morpholinos used.

RNA extraction and RT-PCR

Total RNA was extracted from either an isolated embryo or several embryos injected with control, Rab8, Rab11 or Rab35 morpholinos using TRIzol reagent. The RT-PCR was performed on each sample using OneTaq One-Step RT-PCR Kit (see key resource table) with the forward primers “tcagtatggcgaagacctacgat”, “gttagcatggctactgcctaatcac”, “gtaatgagcgactgactgctgac” and reverse primers “tcttcacagtagcacacagcga”, “catgtcattgtctcggcggtc”, “gtgcaaggagaaaaataagatcaagttagagaatca” for Rab8, Rab11 and Rab35 consecutively. RT-PCR reaction was run using the following cycling conditions: 48 °C for 30 min, 94 °C for 1min followed by 40 cycles of 94 °C for 15 sec, 54 °C (Rab8 and Rab11) or 53 °C (Rab35) for 30 sec, 68 °C for 2 minutes with final extension at 68 °C for 5 min.

Immunofluorescence

Fluorescent transgenic and/or mRNA injected embryos (refer to strains and mRNAs in key resource table, and for injection protocols refer to (Rathbun *et al.*, 2020a; Aljiboury *et al.*, 2021)) were staged at Kupffer’s Vesicle (KV) developmental stages as described in (Amack *et al.*, 2007; Rathbun *et al.*, 2020b) and fixed using 4% paraformaldehyde with 0.1% triton-100. Standard immunofluorescent protocols were carried out (refer to (Aljiboury *et al.*, 2021)). Embryos were then embedded in low-melting 2% agarose (see key resource table) with the KV positioned at the bottom of a #1.5 glass bottom MatTek plate (see key resource table) and imaged using the spinning disk confocal microscope or LSCM (see details below).

Imaging

Zebrafish embryos were imaged using Leica DMi8 (Leica, Bannockburn, IL) equipped with a X-light V2 Confocal unit spinning disk equipped with a Visitron VisiFRAP-DC photokinetics unit, a Leica SP8 (Leica, Bannockburn, IL) laser scanner confocal microscope (LSCM) and/or a Zeiss LSM 980 (Carl Zeiss, Germany) with Airyscan 2 confocal microscope. The Leica DMi8 is equipped with a Lumencore SPECTRA X (Lumencore, Beaverton, OR), Photometrics Prime-95B sCMOS Camera, and 89 North-LDi laser launch. VisiView software was used to acquire images. Optics used with this unit are HC PL APO x40/1.10W CORR CS2 0.65 water immersion objective, HC PL APO x40/0.95 NA CORR dry and HCX PL APO x63/1.40-0.06 NA oil objective. The SP8 laser scanning confocal microscope is equipped with HC PL APO 20x/0.75 IMM CORR CS2 objective, HC PL APO 40x/1.10 W CORR CS2 0.65 water objective and HC PL APO x63/1.3 Glyc CORR CS2 glycerol objective. LAS-X software was used to acquire images. The Zeiss LSM 980 is equipped with a T-PMT, GaASP detector, MA-PMT, Airyscan 2 multiplex with 4Y and 8Y. Optics used with this unit are PL APO x63/1.4 NA oil DIC. Zeiss Zen 3.2 was used to acquire the images. A Leica M165 FC stereomicroscope equipped with DFC 9000 GT sCMOS camera was used for staging and phenotypic analysis of zebrafish embryos.

Optogenetic experiments in zebrafish embryos

Tg(sox17:GFP-CAAX), Tg*BAC*(cftr-GFP), Tg(sox17:GFP), Tg(sox17:DsRed) and TgKIeGFP-Rab11a zebrafish embryos were injected with 50-100 pg of CRY2 and/or CIB1-mCherry-Rab11, CIB1-mCherry-Rab8 or CIB1-mRuby-Rab35 at the one cell to 4 cell stage. Embryos were allowed to develop in the dark until uninjected embryos reached the 75% epiboly stage where we can screen embryos for KV cells and expose them to 488nm light using the NIGHTSEA fluorescence system until the six-somite stage (Rathbun *et al.*, 2020b). Embryos were then fixed and immunostained (refer to (Aljiboury *et al.*, 2021).

Analysis of Zebrafish developmental defects and heart looping defects following acute optogenetic clustering

Zebrafish embryos injected with optogenetic constructs were exposed to 488nm light from 8 hpf-12 hpf as described in Rathbun et al., 2020. Embryos were incubated at 28.5°C until 42 hpf. Zebrafish were manually dechorionated using forceps and mounted in 2% agarose before imaging. Heart loop assessment and imaging were carried out on Leica M165 FC stereomicroscope equipped with DFC 9000 GT sCMOS29camera. A Plan Apochromat 1X objective and GFP excitation emission filter was used. Images were acquired using LAS-X software and post-image processing was done using thunder imaging system from Leica. Lateral view and ventral view of zebrafish were obtained from bright field imaging. Time lapse video of heart looping was performed at 0.25 seconds interval. Heart looping was characterized by leftward, rightward and severely defective looping. Gross embryo phenotypes were categorized into no tail, curved tail, and single eye phenotypes. Categorization was performed over 787 embryos over n>3 clutches with at least 88-274 embryos per condition.

Image and data analysis

Images were processed using FIJI/ImageJ. Graphs and statistical analysis were produced using Prism 9 software. Surface rendering (refer to (Rathbun *et al.*, 2020b)) and analysis of KV cells were performed using Bitplane IMARIS software. Videos were created using FIJI/ImageJ or IMARIS. Cilia length was measured as the distance from the base of the cilia to the tip using line function in IMARIS. For percentage of ciliated KV cells, the number of cells with cilia was counted and represented as a percentage over the total number of cells in the cyst forming tissue.

Relative cilia distance from cell border closest to KV center: the distance from cilia to the cell membrane closest to KV center (l2) was measured and divided by the distance of the center of the cell (nucleus) to the cell's membrane closes to KV center(l1); d=l2/l1. This was done for KV cells with positive cilia staining at each developmental KV stage.

Ratio of junctional to apical localization: Using imageJ/FIJI a box was drawn on the cell-cell junction and the mean intensity for the required channel was obtained. The same sized box was drawn on the apical membrane and the mean intensity was obtained. The ratio between the junctional and apical mean intensities were then obtained for four cells within the acquired timelapse movie for an embryo across developmental KV time points that included the rosette, early lumen, and late lumen stages.

Calculating colocalization of actin, CFTR, and Rab GTPases with select optogenetic clusters: From fixed embryos the total number of Rab GTPase clusters were counted for each KV. The number of Rab clusters that had CFTR, actin, or Rab GTPase being tested overlapping with the Rab GTPase cluster was counted and presented as a percentage.

Statistical Analysis

Unpaired two-tailed t-tests and one way ANOVA were performed using PRISM9 software. **** denotes a p-value<0.0001, *** p-value<0.001, **p-value<0.01, *p-value<0.05, n.s. not significant. For further information on detailed statistical analysis see supplemental table 1.

REFERENCES CITED

Aljiboury, AA, Mujcic, A, Cammerino, T, Rathbun, LI, and Hehnly, H (2021). Imaging the early zebrafish embryo centrosomes following injection of small-molecule inhibitors to understand spindle formation. STAR Protoc 2, 100293.

Amack, JD, Wang, X, and Yost, HJ (2007). Two T-box genes play independent and cooperative roles to regulate morphogenesis of ciliated Kupffer's vesicle in zebrafish. Dev Biol 310, 196–210.

Amack, JD, and Yost, HJ (2004). The T box transcription factor no tail in ciliated cells controls zebrafish left-right asymmetry. Curr Biol 14, 685–690.

Belicova, L, Repnik, U, Delpierre, J, Gralinska, E, Seifert, S, Valenzuela, JI, Morales-Navarrete, HA, Franke, C, Räägel, H, Shcherbinina, E, et al. (2021). Anisotropic expansion of hepatocyte lumina enforced by apical bulkheads. J Cell Biol 220.

Borchers, AC, Langemeyer, L, and Ungermann, C (2021). Who's in control? Principles of Rab GTPase activation in endolysosomal membrane trafficking and beyond. J Cell Biol 220.

Bryant, DM, Datta, A, Rodríguez-Fraticelli, AE, PeräCurrency Signnen, J, Martín-Belmonte, F, and Mostov, KE (2010). A molecular network for de novo generation of the apical surface and lumen. Nat Cell Biol 12, 1035–1045.

Compagnon, J, Barone, V, Rajshekar, S, Kottmeier, R, Pranjic-Ferscha, K, Behrndt, M, and Heisenberg, CP (2014). The notochord breaks bilateral symmetry by controlling cell shapes in the zebrafish laterality organ. Dev Cell 31, 774–783.

Cuenca, A, Insinna, C, Zhao, H, John, P, Weiss, MA, Lu, Q, Walia, V, Specht, S, Manivannan, S, Stauffer, J, et al. (2019). The C7orf43/TRAPPC14 component links the TRAPPII complex to Rabin8 for preciliary vesicle tethering at the mother centriole during ciliogenesis. J Biol Chem 294, 15418–15434.

Demir, K, Kirsch, N, Beretta, CA, Erdmann, G, Ingelfinger, D, Moro, E, Argenton, F, Carl, M, Niehrs, C, and Boutros, M (2013). RAB8B Is Required for Activity and Caveolar Endocytosis of LRP6. Cell Rep 4, 1224–1234.

Essner, JJ, Amack, JD, Nyholm, MK, Harris, EB, and Yost, HJ (2005). Kupffer's vesicle is a ciliated organ of asymmetry in the zebrafish embryo that initiates left-right development of the brain, heart and gut. Development 132, 1247–1260.

Feldman, JL, and Priess, JR (2012). A role for the centrosome and PAR-3 in the hand-off of MTOC function during epithelial polarization. Curr Biol 22, 575–582.

Ganga, AK, Kennedy, MC, Oguchi, ME, Gray, S, Oliver, KE, Knight, TA, De La Cruz, EM, Homma, Y, Fukuda, M, and Breslow, DK (2021). Rab34 GTPase mediates ciliary membrane formation in the intracellular ciliogenesis pathway. Curr Biol 31, 2895-2905.e7.

Gokey, JJ, Ji, Y, Tay, HG, Litts, B, and Amack, JD (2016). Kupffer's vesicle size threshold for robust left-right patterning of the zebrafish embryo. Dev Dyn 245, 22–33.

Grimes, DT, and Burdine, RD (2017). Left–Right Patterning: Breaking Symmetry to Asymmetric Morphogenesis. Trends Genet 33, 616–628.

Hall, NA, and Hehnly, H (2021). A centriole's subdistal appendages: contributions to cell division, ciliogenesis and differentiation. Open Biol 11, 200399.

Homma, Y, Hiragi, S, and Fukuda, M (2021). Rab family of small GTPases: an updated view on their regulation and functions. FEBS J 288, 36–55.

Kimmel, CB, Ballard, WW, Kimmel, SR, Ullmann, B, and Schilling, TF (1995). Stages of embryonic development of the zebrafish. Dev Dyn 203, 253–310.

Klinkert, K, Rocancourt, M, Houdusse, A, and Echard, A (2016). Rab35 GTPase couples cell division with initiation of epithelial apico-basal polarity and lumen opening. Nat Commun 7.

Knödler, A, Feng, S, Zhang, J, Zhang, X, Das, A, Peränen, J, and Guo, W (2010). Coordination of Rab8 and Rab11 in primary ciliogenesis. Proc Natl Acad Sci U S A 107, 6346–6351.

Krishnan, N, Swoger, M, Rathbun, LI, Fioramonti, PJ, Freshour, J, Bates, M, Patteson, AE, and Hehnly, H (2022). Rab11 endosomes and Pericentrin coordinate centrosome movement during pre-abscission in vivo. Life Sci Alliance 5, 1–15.

Kuhns, S, Seixas, C, Pestana, S, Tavares, B, Nogueira, R, Jacinto, R, Ramalho, JS, Simpson, JC, Andersen, JS, Echard, A, et al. (2019). Rab35 controls cilium length, function and membrane composition. EMBO Rep 20.

Levic, DS, Yamaguchi, N, Wang, S, Knaut, H, and Bagnat, M (2021). Knock-in tagging in zebrafish facilitated by insertion into non-coding regions. 148, 2021.07.08.451679.

Lindsay, AJ, Jollivet, F, Horgan, CP, Khan, AR, Raposo, G, McCaffrey, MW, and Goud, B (2013). Identification and characterization of multiple novel Rab-myosin Va interactions. Mol Biol Cell 24, 3420–3434.

Lu, Q, Insinna, C, Ott, C, Stauffer, J, Pintado, PA, Rahajeng, J, Baxa, U, Walia, V, Cuenca, A, Hwang, YS, et al. (2015). Early steps in primary cilium assembly require EHD1/EHD3-dependent ciliary vesicle formation. Nat Cell Biol 17, 228–240.

Melby, AE, Warga, RM, and Kimmel, CB (1996). Specification of cell fates at the dorsal margin of the zebrafish gastrula. Development 122, 2225–2237.

Moreno-Ayala, R, Olivares-Chauvet, P, Schäfer, R, and Junker, JP (2021). Variability of an Early Developmental Cell Population Underlies Stochastic Laterality Defects. Cell Rep 34.

Naslavsky, N, and Caplan, S (2020). Endocytic membrane trafficking in the control of centrosome function.

Navis, A, Marjoram, L, and Bagnat, M (2013). Cftr controls lumen expansion and function of Kupffer's vesicle in zebrafish. Development 140, 1703–1712.

Nguyen, MK, Kim, CY, Kim, JM, Park, BO, Lee, S, Park, H, and Heo, W Do (2016). Optogenetic oligomerization of Rab GTPases regulates intracellular membrane trafficking. Nat Chem Biol 12, 431–436.

Oguchi, ME, Okuyama, K, Homma, Y, and Fukuda, M (2020). A comprehensive analysis of Rab GTPases reveals a role for Rab34 in serum starvation-induced primary ciliogenesis. J Biol Chem 295, 12674.

Omori, Y, Zhao, C, Saras, A, Mukhopadhyay, S, Kim, W, Furukawa, T, Sengupta, P, Veraksa, A, and Malicki, J (2008). Elipsa is an early determinant of ciliogenesis that links the IFT particle to membrane-associated small GTPase Rab8. Nat Cell Biol 10, 437–444.

Oteíza, P, Köppen, M, Concha, ML, and Heisenberg, CP (2008). Origin and shaping of the laterality organ in zebrafish. Development 135, 2807–2813.

Rathbun, LI, Aljiboury, AA, Bai, X, Hall, NA, Manikas, J, Amack, JD, Bembenek, JN, and Hehnly, H (2020a). PLK1- and PLK4-Mediated Asymmetric Mitotic Centrosome Size and Positioning in the Early Zebrafish Embryo. Curr Biol 30, 4519-4527.e3.

Rathbun, LI, Colicino, EG, Manikas, J, O'Connell, J, Krishnan, N, Reilly, NS, Coyne, S, Erdemci-Tandogan, G, Garrastegui, AM, Freshour, J, et al. (2020b). Cytokinetic bridge triggers de novo lumen formation in vivo. Nat Commun 11, 1–12.

Saydmohammed, M, Yagi, H, Calderon, M, Clark, MJ, Feinstein, T, Sun, M, Stolz, DB, Watkins, SC, Amack, JD, Lo, CW, et al. (2018). Vertebrate myosin 1d regulates left–right organizer morphogenesis and laterality. Nat Commun 9.

SOROKIN, S (1962). Centrioles and the formation of rudimentary cilia by fibroblasts and smooth muscle cells. J Cell Biol 15, 363–377.

Sorokin, SP (1968). Reconstructions of centriole formation and ciliogenesis in mammalian lungs. J Cell Sci 3, 207–230.

Vertii, A, Bright, A, Delaval, B, Hehnly, H, and Doxsey, S (2015). New frontiers: discovering cilia-independent functions of cilia proteins. EMBO Rep 16, 1275–1287.

Vertii, A, Hehnly, H, and Doxsey, S (2016). The centrosome, a multitalented renaissance organelle. Cold Spring Harb Perspect Biol 8.

Wang, G, Cadwallader, AB, Jang, DS, Tsang, M, Yost, HJ, and Amack, JD (2011). The Rho kinase rock2b establishes anteroposterior asymmetry of the ciliated Kupffer's vesicle in zebrafish. Development 138, 45–54.

Warga, RM, and Nüsslein-Volhard, C (1999). Origin and development of the zebrafish endoderm. Development 126, 827–838.

Westlake, CJ, Baye, LM, Nachury, M V., Wright, KJ, Ervin, KE, Phu, L, Chalouni, C, Beck, JS, Kirkpatrick, DS, Slusarski, DC, et al. (2011). Primary cilia membrane assembly is initiated by Rab11 and transport protein particle II (TRAPPII) complex-dependent trafficking of Rabin8 to the centrosome. Proc Natl Acad Sci U S A 108, 2759–2764.

Willoughby, PM, Allen, M, Yu, J, Korytnikov, R, Chen, T, Liu, Y, So, I, Macpherson, N, Mitchell, JA, Fernandez-Gonzalez, R, et al. (2021). The recycling endosome protein Rab25 coordinates collective cell movements in the zebrafish surface epithelium. Elife 10.

Wu, C-T, Chen, H-Y, and Tang, TK (2018). Myosin-Va is required for preciliary vesicle transportation to the mother centriole during ciliogenesis. Nat Cell Biol 20, 175–185.

Yoshimura, SI, Egerer, J, Fuchs, E, Haas, AK, and Barr, FA (2007). Functional dissection of Rab GTPases involved in primary cilium formation. 178, 363–369.

Zhang, H, Gao, Y, Qian, P, Dong, Z, Hao, W, Liu, D, and Duan, X (2019). Expression analysis of Rab11 during zebrafish embryonic development. BMC Dev Biol 19, 1–8.

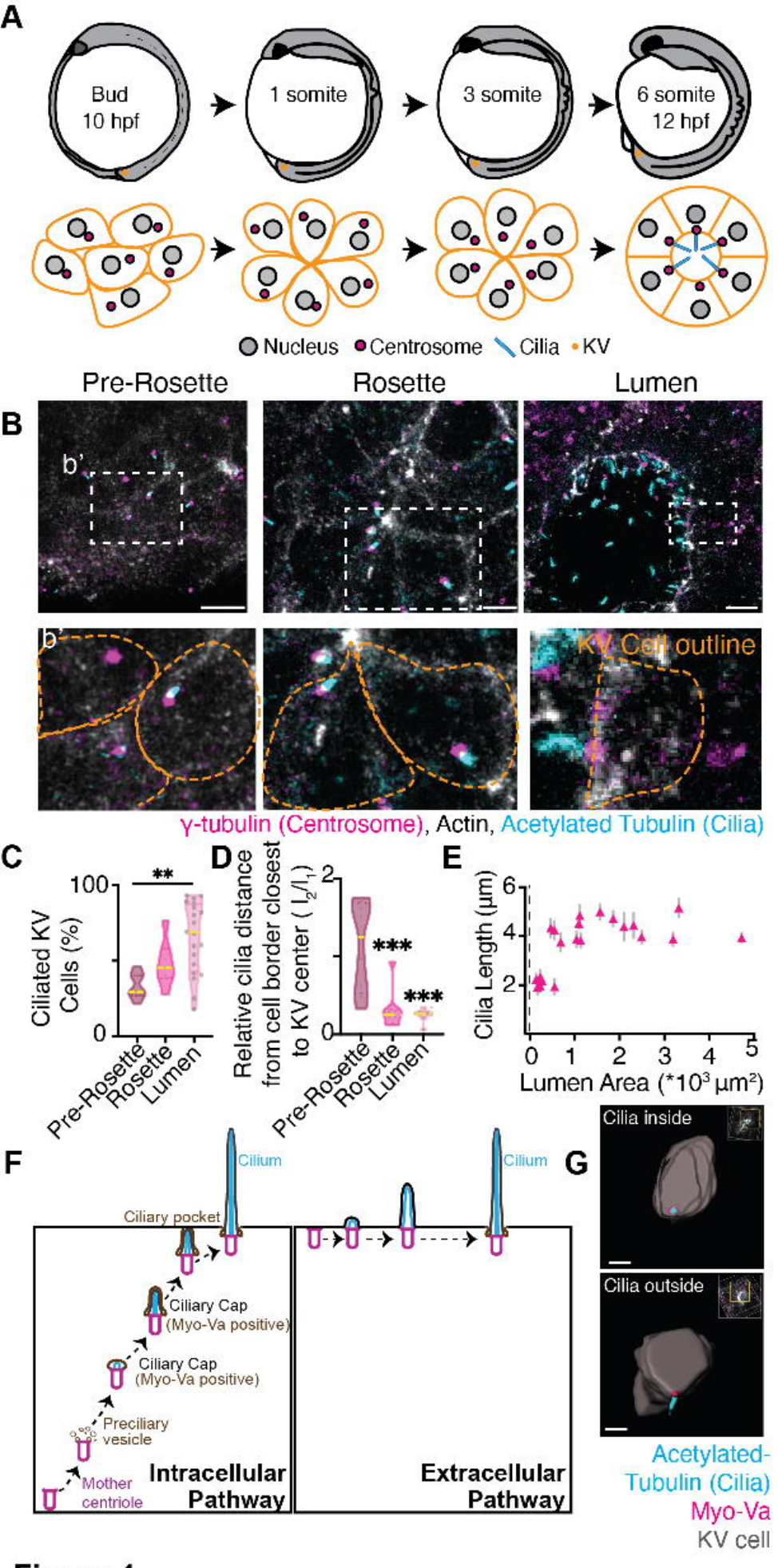
A
Bud
10 hpf
1 somite
3 somite
6 somite
12 hpf
Nucleus
Centrosome
Cilia
KV
Pre-Rosette
Rosette
Lumen
B
b'
KV Cell outline
γ-tubulin (Centrosome), Actin, Acetylated Tubulin (Cilia)
C
Ciliated KV Cells (%)
100
0
**
Pre-Rosette
Rosette
Lumen
D
Relative cilia distance from cell border closest to KV center (l2/l1)
2
0
***
***
Pre-Rosette
Rosette
Lumen
E
Cilia Length (µm)
6
4
2
0
1
2
3
4
5
Lumen Area (*10³ µm²)
F
Cilium
Cilium
Ciliary pocket
Ciliary Cap
(Myo-Va positive)
Ciliary Cap
(Myo-Va positive)
Preciliary
vesicle
Mother
centriole
Intracellular
Pathway
Extracellular
Pathway
G
Cilia inside
Cilia outside
Acetylated-
Tubulin (Cilia)
Myo-Va
KV cell

Figure 1.

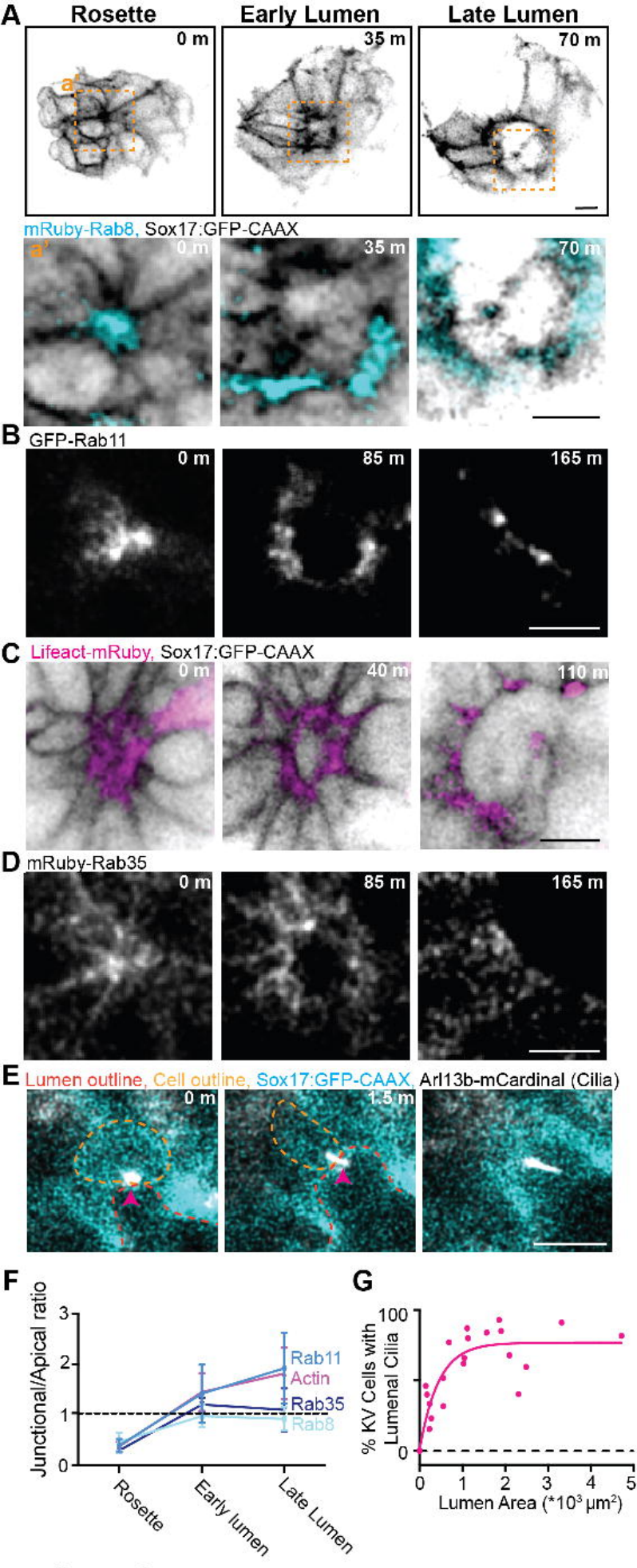
A
Rosette
Early Lumen
Late Lumen
0 m
35 m
70 m
a'
mRuby-Rab8, Sox17:GFP-CAAX
B
GFP-Rab11
0 m
85 m
165 m
C
Lifeact-mRuby, Sox17:GFP-CAAX
0 m
40 m
110 m
D
mRuby-Rab35
0 m
85 m
165 m
E
Lumen outline, Cell outline, Sox17:GFP-CAAX, Arl13b-mCardinal (Cilia)
0 m
1.5 m
F
Junctional/Apical ratio
Rab11
Actin
Rab35
Rab8
Rosette
Early lumen
Late Lumen
G
% KV Cells with Lumenal Cilia
Lumen Area (*10³ µm²)

Figure 2.

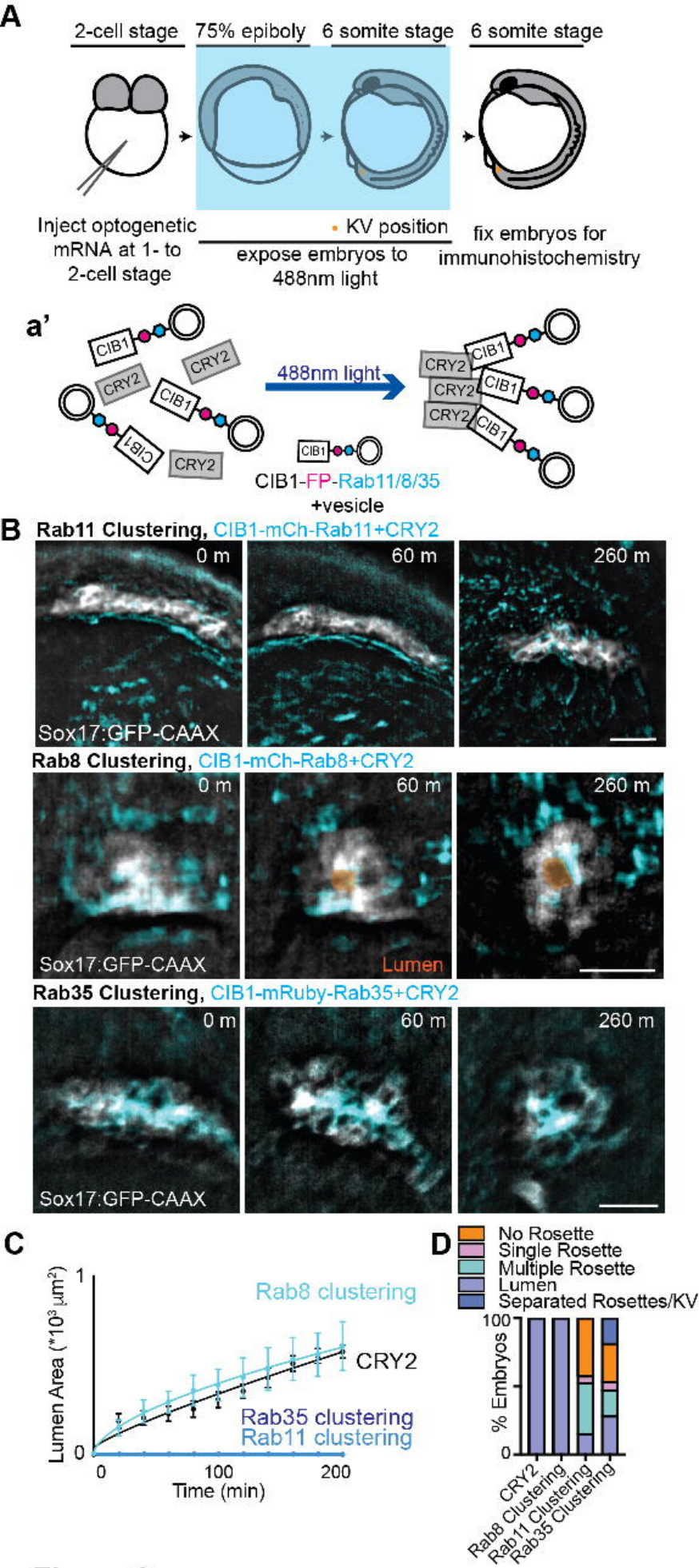
A
2-cell stage
75% epiboly
6 somite stage
6 somite stage
Inject optogenetic mRNA at 1- to 2-cell stage
KV position
expose embryos to 488nm light
fix embryos for immunohistochemistry
a'
CIB1
CRY2
488nm light
CIB1-FP-Rab11/8/35
+vesicle
B
Rab11 Clustering, CIB1-mCh-Rab11+CRY2
0 m
60 m
260 m
Sox17:GFP-CAAX
Rab8 Clustering, CIB1-mCh-Rab8+CRY2
Lumen
Rab35 Clustering, CIB1-mRuby-Rab35+CRY2
C
Lumen Area (*10³ µm²)
Time (min)
Rab8 clustering
CRY2
Rab35 clustering
Rab11 clustering
D
No Rosette
Single Rosette
Multiple Rosette
Lumen
Separated Rosettes/KV
% Embryos
CRY2
Rab8 Clustering
Rab11 Clustering
Rab35 Clustering

Figure 3.

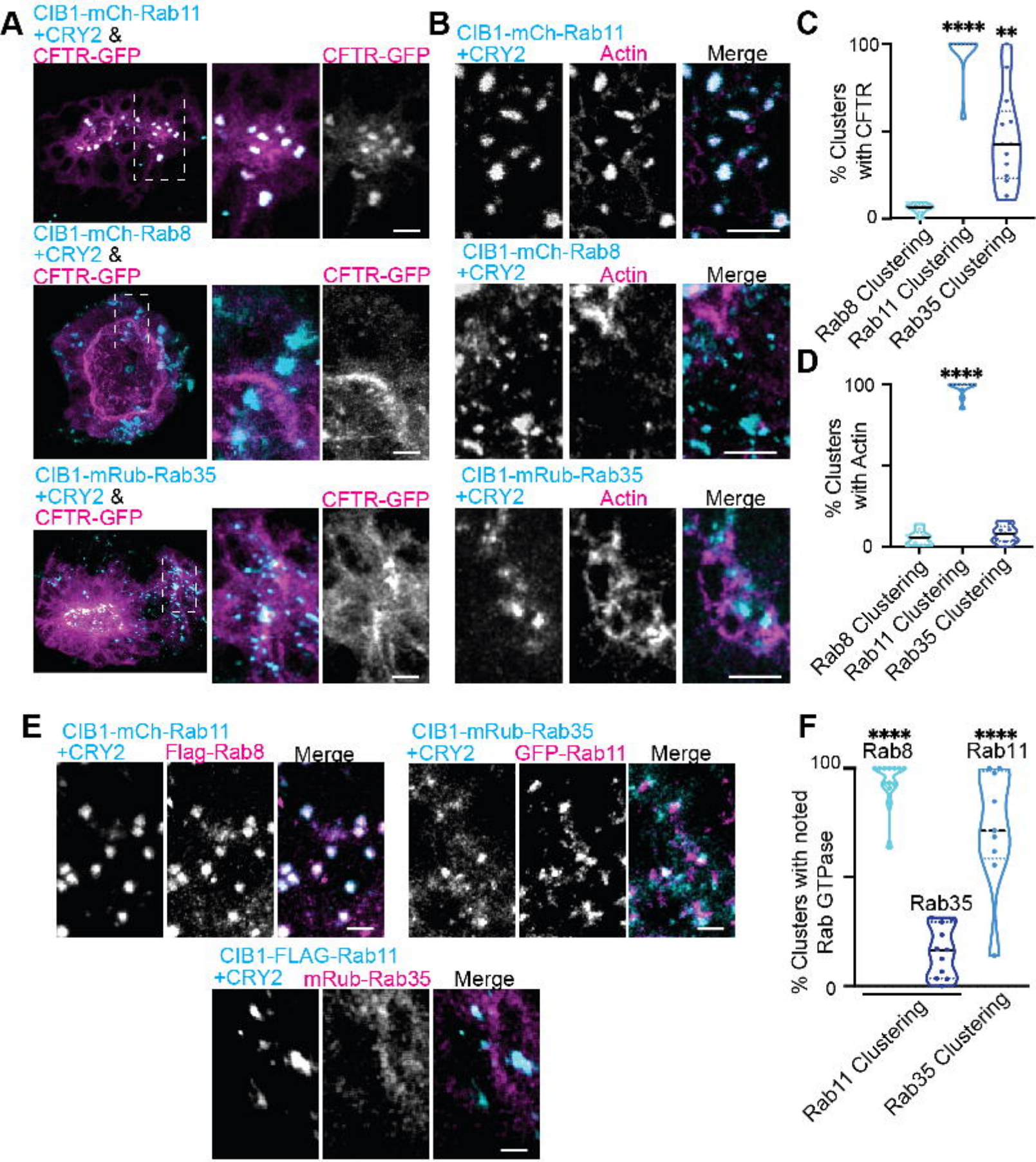
A
CIB1-mCh-Rab11
+CRY2 &
CFTR-GFP
CFTR-GFP
CIB1-mCh-Rab8
+CRY2 &
CFTR-GFP
CFTR-GFP
CIB1-mRub-Rab35
+CRY2 &
CFTR-GFP
CFTR-GFP
B
CIB1-mCh-Rab11
+CRY2
Actin
Merge
CIB1-mCh-Rab8
+CRY2
Actin
Merge
CIB1-mRub-Rab35
+CRY2
Actin
Merge
C
****
**
100
0
% Clusters
with CFTR
Rab8 Clustering
Rab11 Clustering
Rab35 Clustering
D
****
100
0
% Clusters
with Actin
Rab8 Clustering
Rab11 Clustering
Rab35 Clustering
E
CIB1-mCh-Rab11
+CRY2
Flag-Rab8
Merge
CIB1-mRub-Rab35
+CRY2
GFP-Rab11
Merge
CIB1-FLAG-Rab11
+CRY2
mRub-Rab35
Merge
F
****
Rab8
****
Rab11
100
0
Rab35
% Clusters with noted
Rab GTPase
Rab11 Clustering
Rab35 Clustering

Figure 4.

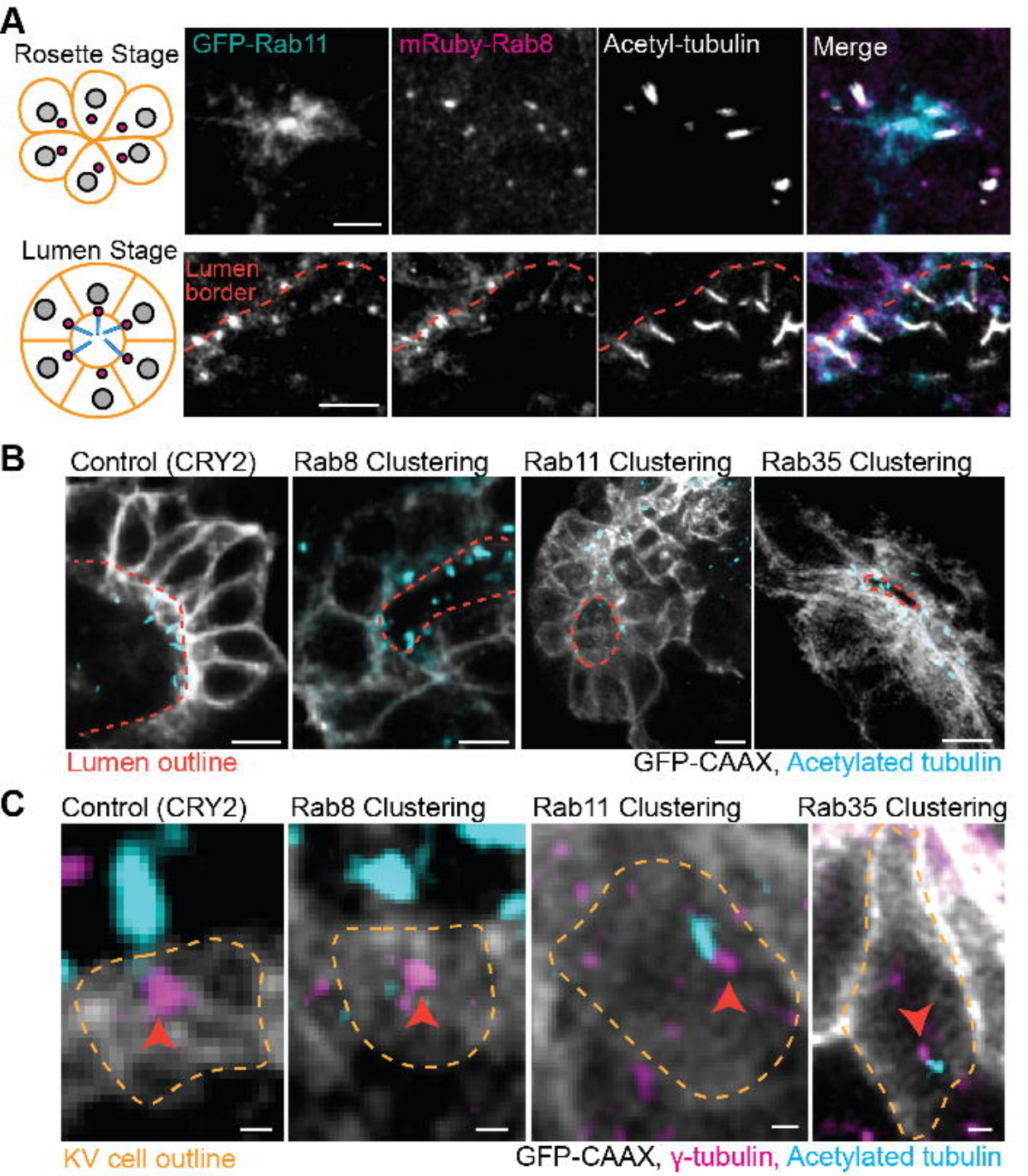
A
Rosette Stage
GFP-Rab11
mRuby-Rab8
Acetyl-tubulin
Merge
Lumen Stage
Lumen border
B
Control (CRY2)
Rab8 Clustering
Rab11 Clustering
Rab35 Clustering
Lumen outline
GFP-CAAX, Acetylated tubulin
C
Control (CRY2)
Rab8 Clustering
Rab11 Clustering
Rab35 Clustering
KV cell outline
GFP-CAAX, γ-tubulin, Acetylated tubulin
D
KV cells with cilia (%)
100
0
n.s.
****
**
CRY2
Rab8 Clustering
Rab11 Clustering
Rab35 Clustering
E
Cilia length (μm)
8
0
****
****
****
CRY2
Rab8 Clustering
Rab11 Clustering
Rab35 Clustering
F
KV cilia in cell volume (%)
50
0
n.s.
**
***
CRY2
Rab8 Clustering
Rab11 Clustering
Rab35 Clustering
G
Cilia distance from cell boarder closest to KV center
3
0
n.s.
****
****
CRY2
Rab8 Clustering
Rab11 Clustering
Rab35 Clustering

Figure 5.

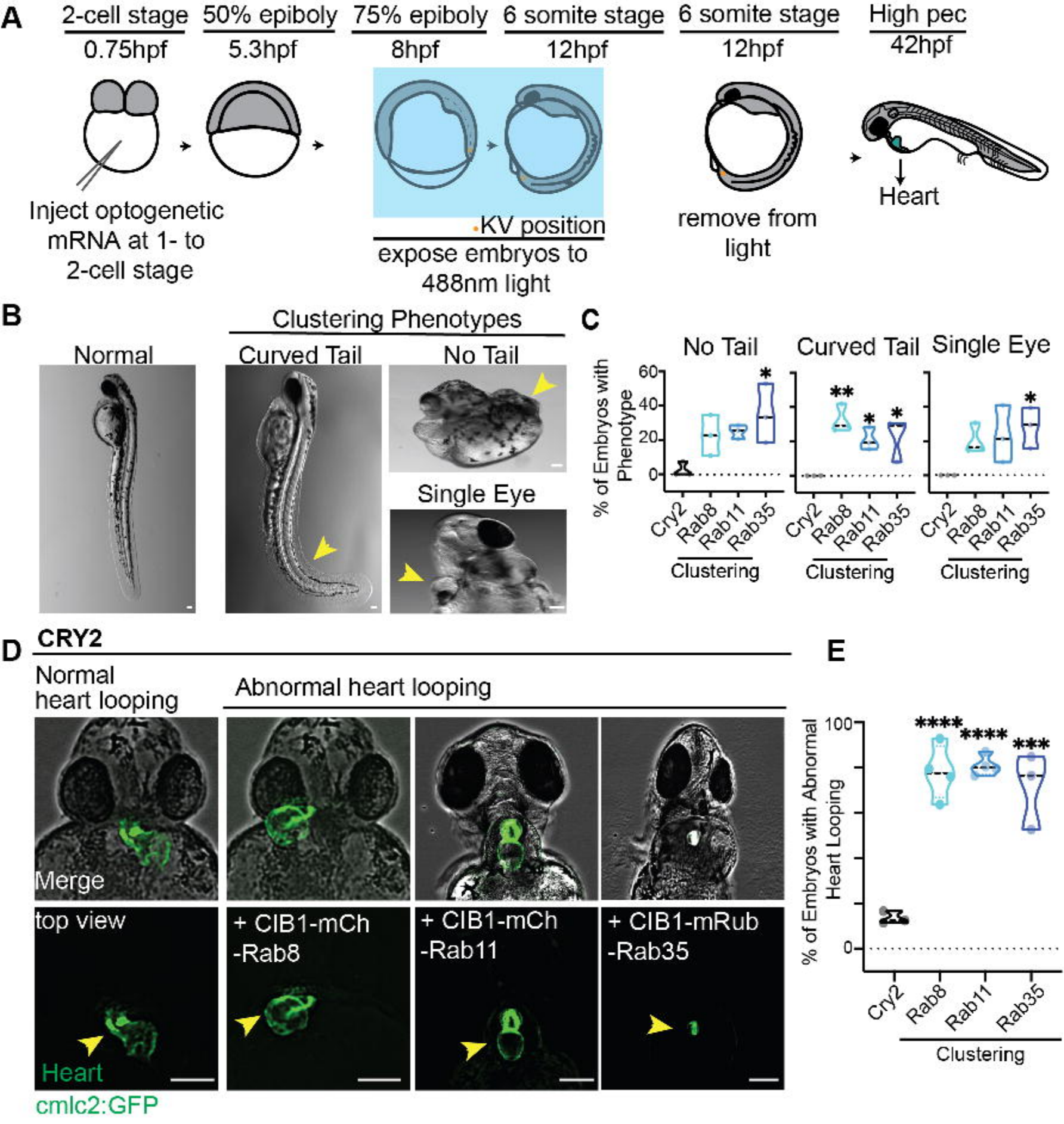
A
2-cell stage
0.75hpf
50% epiboly
5.3hpf
75% epiboly
8hpf
6 somite stage
12hpf
6 somite stage
12hpf
High pec
42hpf
Inject optogenetic mRNA at 1- to 2-cell stage
KV position
expose embryos to 488nm light
remove from light
Heart
B
Clustering Phenotypes
Normal
Curved Tail
No Tail
Single Eye
C
No Tail
Curved Tail
Single Eye
% of Embryos with Phenotype
Cry2
Rab8
Rab11
Rab35
Clustering
D
CRY2
Normal heart looping
Abnormal heart looping
Merge
top view
+ CIB1-mCh -Rab8
+ CIB1-mCh -Rab11
+ CIB1-mRub -Rab35
Heart
cmlc2:GFP
E
% of Embryos with Abnormal Heart Looping
Cry2
Rab8
Rab11
Rab35
Clustering

Figure 6.

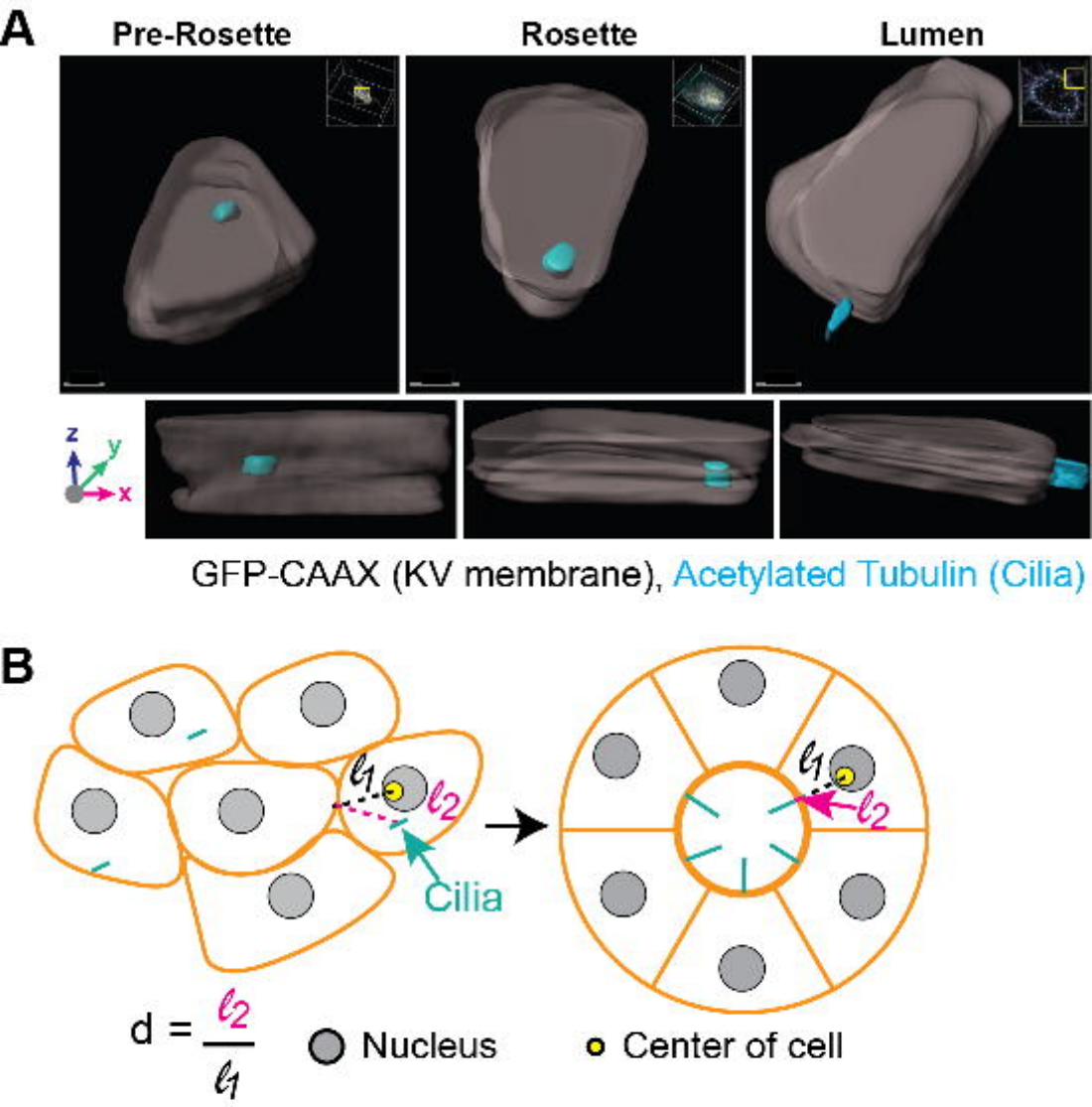
A
Pre-Rosette
Rosette
Lumen
z
y
x
GFP-CAAX (KV membrane), Acetylated Tubulin (Cilia)
B
ℓ_1
ℓ_2
Cilia
$d = \frac{\ell_2}{\ell_1}$
Nucleus
Center of cell

Figure S1.

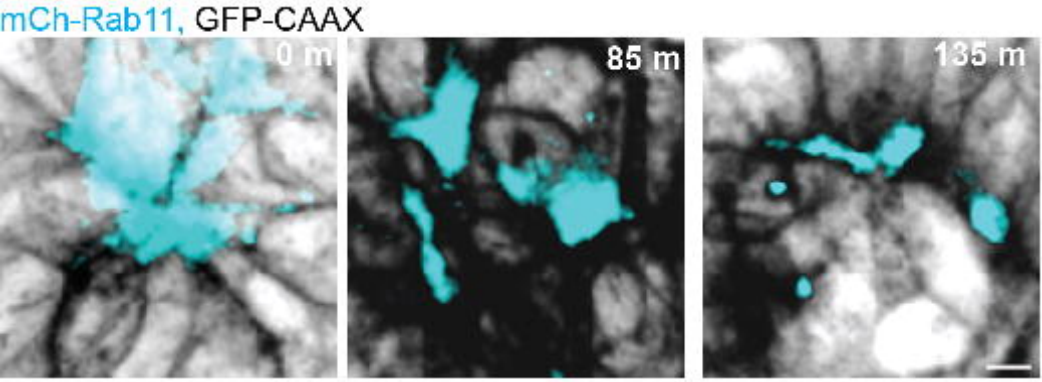

Figure S2.

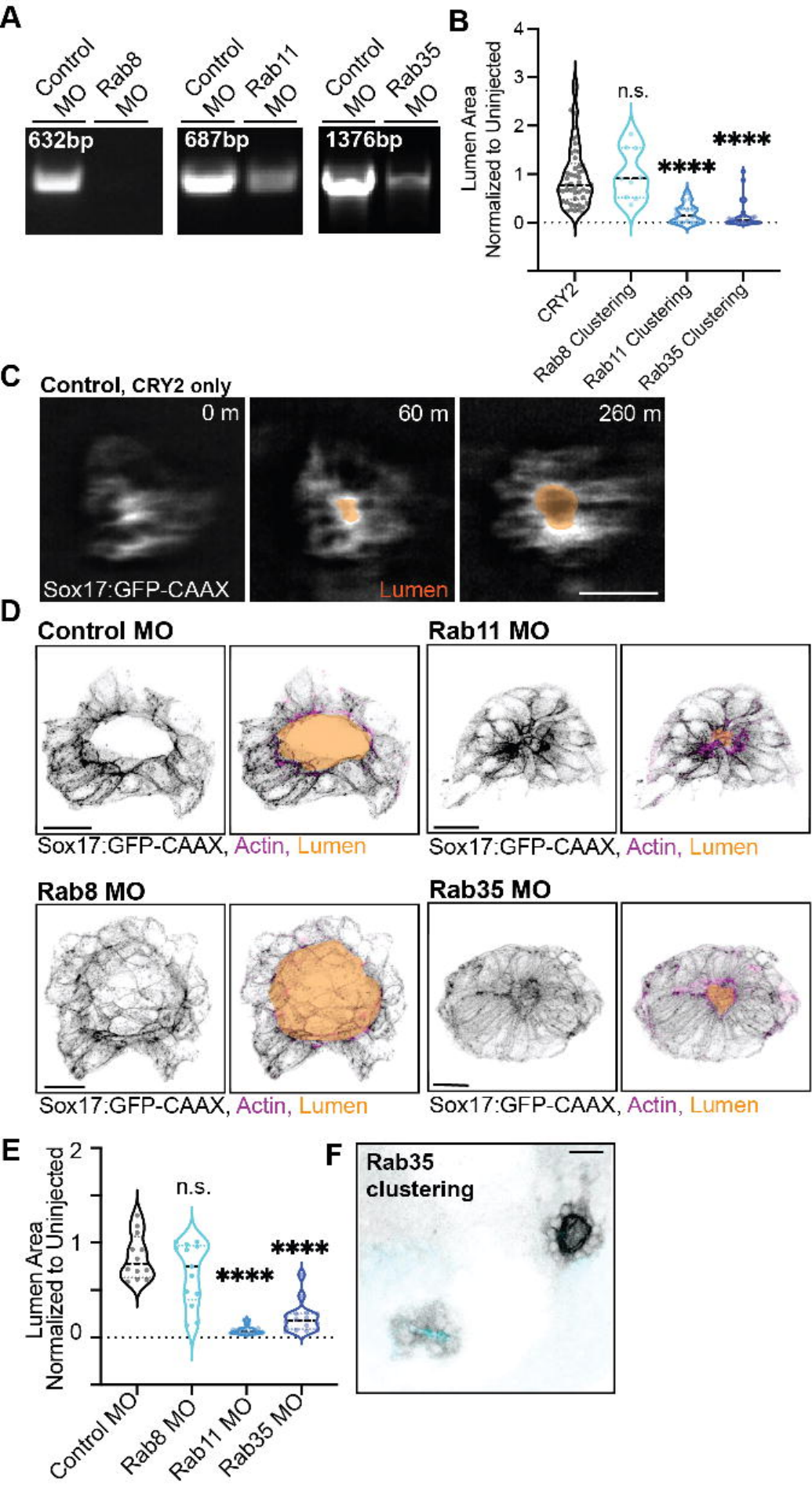
A
Control MO
Rab8 MO
632bp
Control MO
Rab11 MO
687bp
Control MO
Rab35 MO
1376bp
B
Lumen Area Normalized to Uninjected
n.s.
****
****
CRY2
Rab8 Clustering
Rab11 Clustering
Rab35 Clustering
C
Control, CRY2 only
0 m
60 m
260 m
Sox17:GFP-CAAX
Lumen
D
Control MO
Rab11 MO
Sox17:GFP-CAAX, Actin, Lumen
Sox17:GFP-CAAX, Actin, Lumen
Rab8 MO
Rab35 MO
Sox17:GFP-CAAX, Actin, Lumen
Sox17:GFP-CAAX, Actin, Lumen
E
Lumen Area Normalized to Uninjected
n.s.
****
****
Control MO
Rab8 MO
Rab11 MO
Rab35 MO
F
Rab35 clustering

Figure S3.

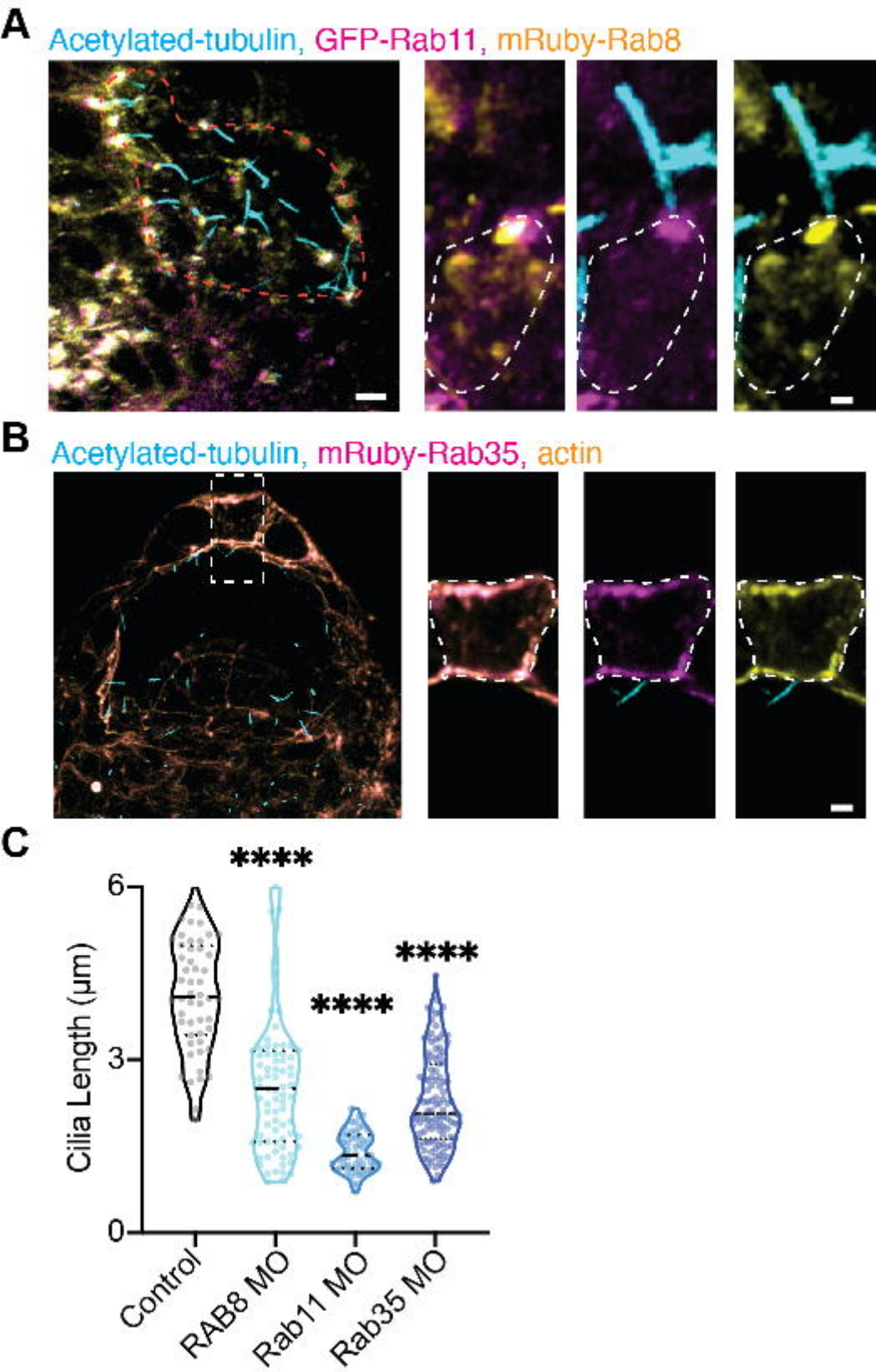
A
Acetylated-tubulin, GFP-Rab11, mRuby-Rab8
B
Acetylated-tubulin, mRuby-Rab35, actin
C
Cilia Length (µm)
6
3
0
****
****
****
Control
RAB8 MO
Rab11 MO
Rab35 MO

Figure S4.